# Global Energetics of Solar Flares and CMEs: Magnetic, Thermal, Non-thermal, and CME energies

**Markus Aschwanden**
**Gordon Holman**
**Yan Xu**
**Ju Jing**
**Paul Boerner**
**Daniel Ryan**
**Amir Caspi**
**James McTiernan**
**Harry Warren**
**Aidan O'Flannagain**
**Eduard Kontar**

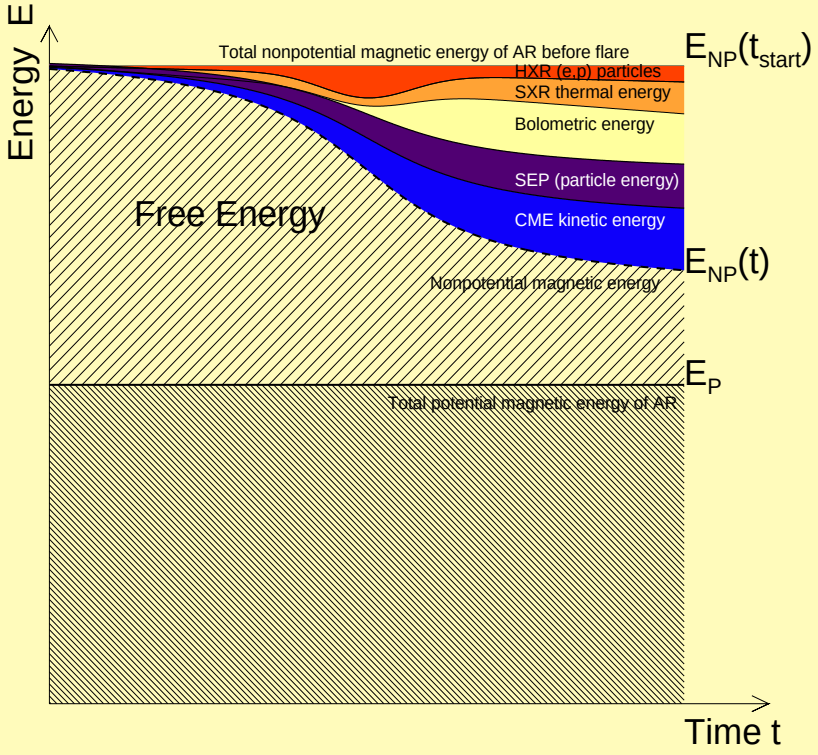


*15th RHESSI Workshop, July 26-30, 2016 University of Graz, Austria*

***http://www.lmsal.com/~aschwand/2016_RHESSI_Graz.ppt***

Publications and Contents of Talk:

(1)Global Energetics of Solar Flares: I. Magnetic Energies",
(Aschwanden, Xu, & Jing 2014, ApJ 797, 50)

(2)Global Energetics of Solar Flares: II. Thermal Energies",
(Aschwanden, Boerner, Ryan, Caspi, McTiernan, Warren,
2015, ApJ 802, 53)

(3)Global Energetics of Solar Flares: III. Nonthermal Energies",
(Aschwanden, Holman, O'Flannagain, Caspi, McTiernan,
& Kontar 2016, ApJ, subm.)

(4)Global Energetics of Solar Flares: IV. Coronal Mass
Ejection Energies, 2016, (Aschwanden, ApJ, subm.)

# What is the Energy Partition in Solar Flares and CMEs?

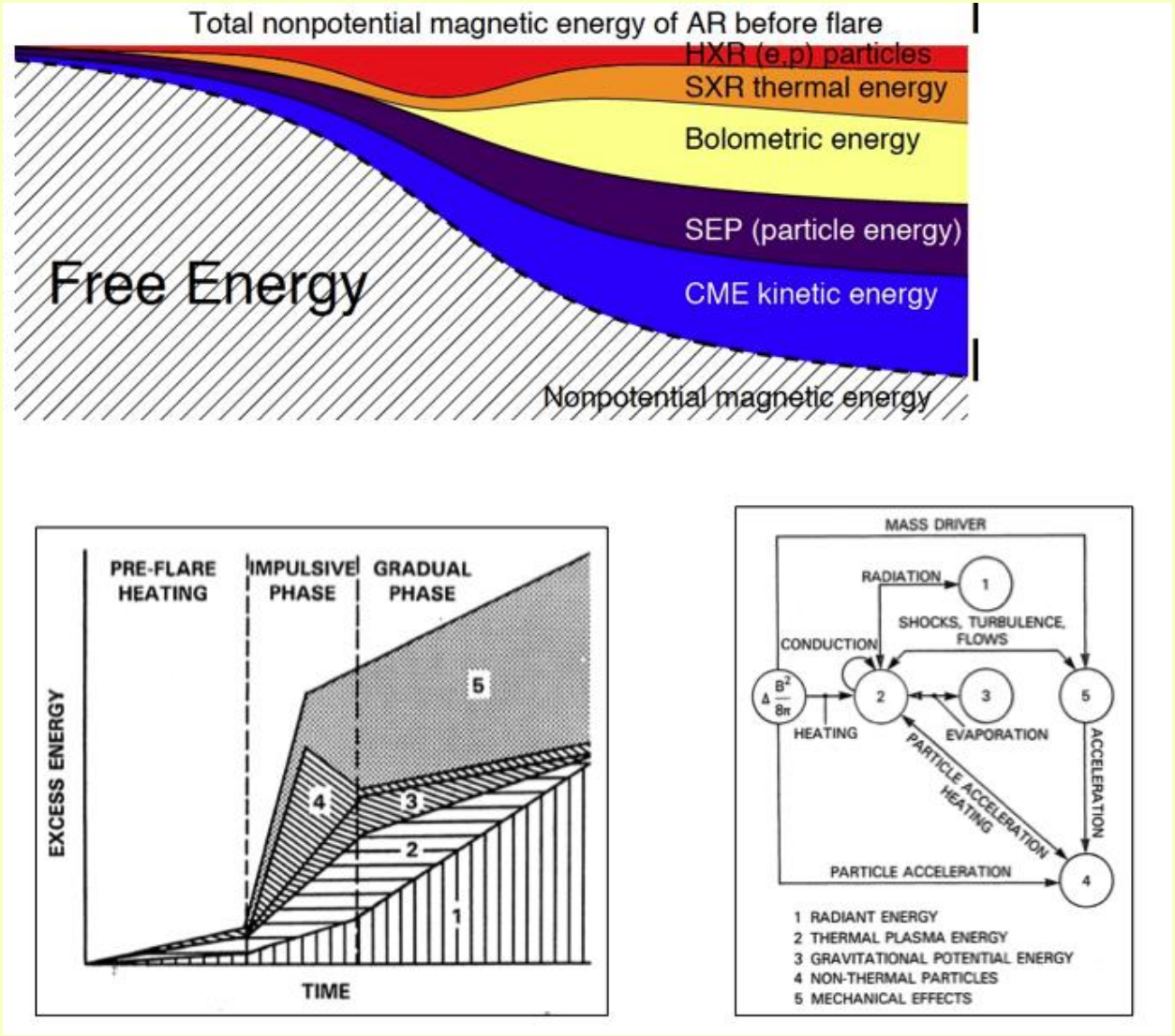


SMM Workshop (Wu et al. 1984, ch. 5)

## Fundamental Questions about Energy Partition in Flares/CMEs:

Does magnetic (reconnection) supply sufficient energy to accelerate (nonthermal) particles ?

$$E_{mag} = (E_{nt} + E_{cme} + \ldots)$$
$$E_{mag} > E_{nt}$$

Is the dissipated magnetic energy in flares sufficient to launch a CME ?

$$E_{mag} > E_{cme}$$
$$E_{cme} = (E_{kin} + E_{grav} + E_{SEP} + \ldots)$$
$$E_{mag} > (E_{kin} + E_{grav})$$

Does the thick-target bremsstrahlung model explain the thermal flare energy ?

$$E_{nt} > E_{th}$$

## Previous study:

## "Global Energetics of 38 large solar eruptive events"

(Emslie et al. 2012, ApJ 559, 71)

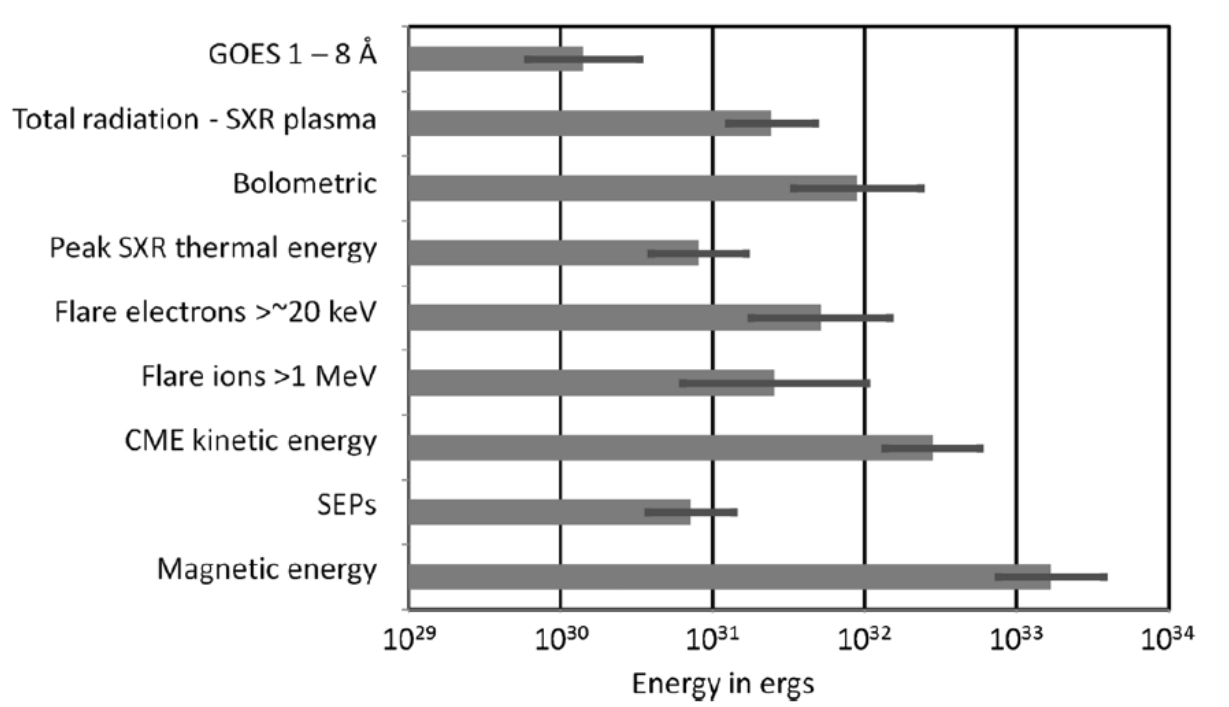


Limitations: (i) no non-potential magnetic field computations
(ii) no imaging (EUV, SXR) data to measure flare areas
(iii) small-number statistics (largest flares only)
(iv) statistically incomplete sampling (above any threshold)
(v) isothermal energy neglects multi-thermality

## Data of SDO Global Energetics Survey Project

Project: Survey on the global energetics of solar flares and CMEs observed with SDO, including data from AIA, HMI, RHESSI, GOES.

Dataset: 2010-2014, first 5 years of SDO mission
399 GOES flares (28 X- and 371 M-class)
177 flares near disk center (<45 deg longitude)

Analysis: 177 flares are suitable for magnetic modeling
FOV=0.25 solar radii
GOES flare start (-0.5 hr) and end time (+0.5 hr)
AIA cadence of 0.1 hr (6 min)
6 AIA filters: 94, 131, 171, 193, 211, 335 A
used for automated loop tracing
AIA pixel size = 0.6”
HMI magnetogram $B_z$ line-of-sight component
HMI pixel size = 0.5” (rebinned by 2 pixels)

# Instrument Coverage for Global Flare Energetics Project

| Energy parameters : | Instruments : | Collaborators : |
|---|---|---|
| Nonpotential magnetic energy | HMI, AIA (NLFFF codes) | Xu, Jing, Aschwanden |
| Potential field magnetic energy | HMI (PFSS or NLFFF codes) | Xu, Jing, Welsch, Aschwanden |
| ... | ... | ... |
| HXR fluence >25 keV | RHESSI | Kontar, O'Flannagain |
| SXR fluence 1-8 A | GOES | Ryan, Aschwanden |
| EUV fluence 94-335 A | AIA | Aschwanden |
| SXR+EUV+UV fluence 1-1060 A | EVE | Woods |
| Bolometric fluence | SORCE | Kretzschmar, C.S.Moore |
| ... | ... | ... |
| EUV peak thermal energy | AIA (DEM), AIA(area) | Aschwanden |
| SXR peak thermal energy | GOES (T, EM), AIA (area) | Ryan |
| SXR+EUV peak thermal energy | GOES+EVE (DEM), AIA (area) | Warren |
| HXR+EUV peak thermal energy | RHESSI+EVE (DEM), AIA (area) | Caspi, McTiernan, Warren |
| ... | ... | ... |
| HXR nonthermal electrons >25 keV | RHESSI | Kontar, O'Flannagain, Guo |
| Gamma-ray producing ions >1 MeV | RHESSI, FERMI | Share, Shih |
| SEP particle energies | ACE, GOES, STEREO | Mewaldt |
| ... | ... | ... |
| CME kinetic + potential energy | COR1+2/STEREO, LASCO/SOHO | Temmer, Vourlidas, Zhang, Warmuth |
| CME thermal energy | STEREO/EUVI, AIA (EUV Dimming, DEM) | Aschwanden, Vourlidas |
| CME thermal energy | UVCS/SOHO | Raymond |
| ... | ... | ... |

# Magnetic Energetics

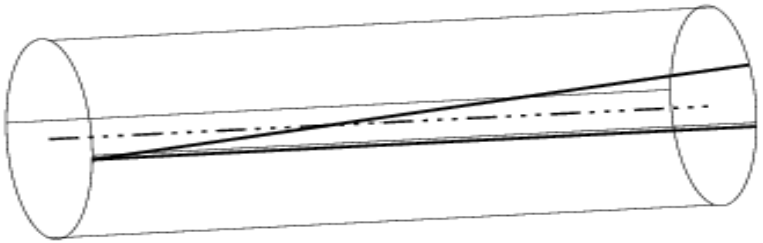

$N_{twist} = 0.1$

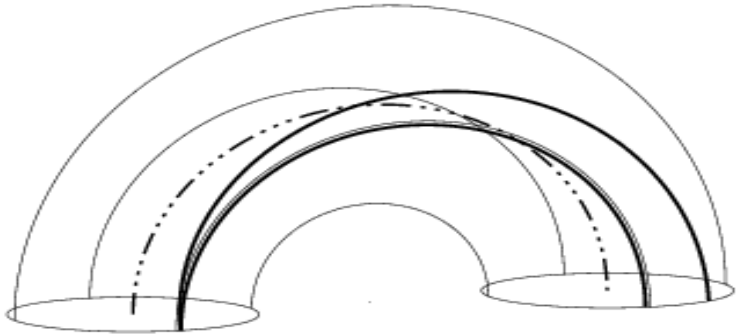

$N_{twist} = 0.1$

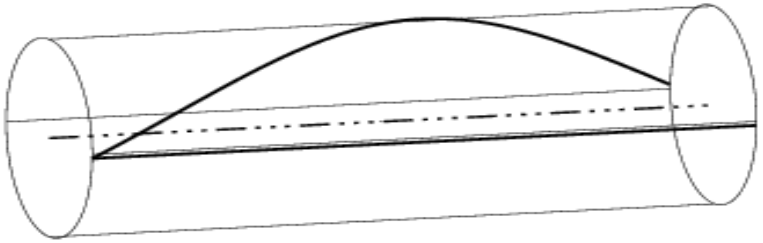

$N_{twist} = 0.5$

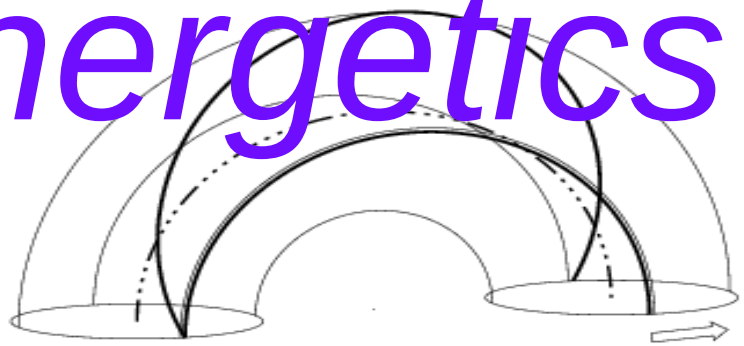

$N_{twist} = 0.5$

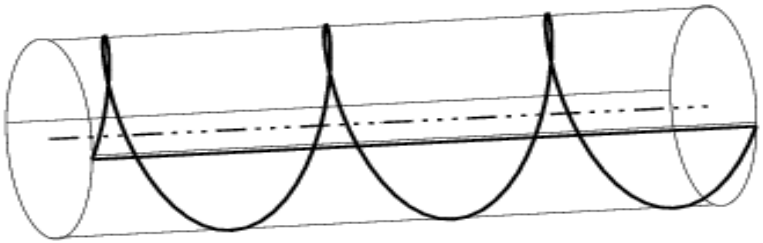

$N_{twist} = 3.0$

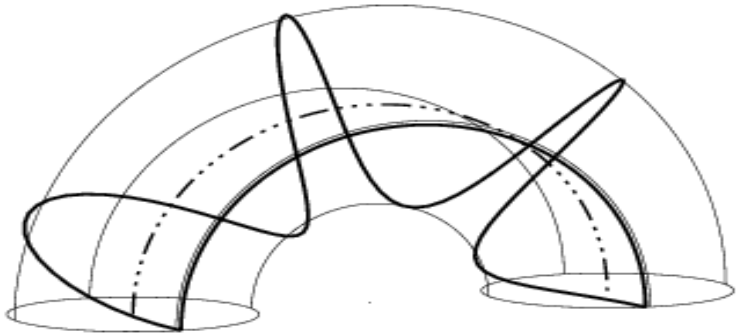

$N_{twist} = 3.0$

# Coronal Non-Linear Force-Free Field Forward-Fitting Method

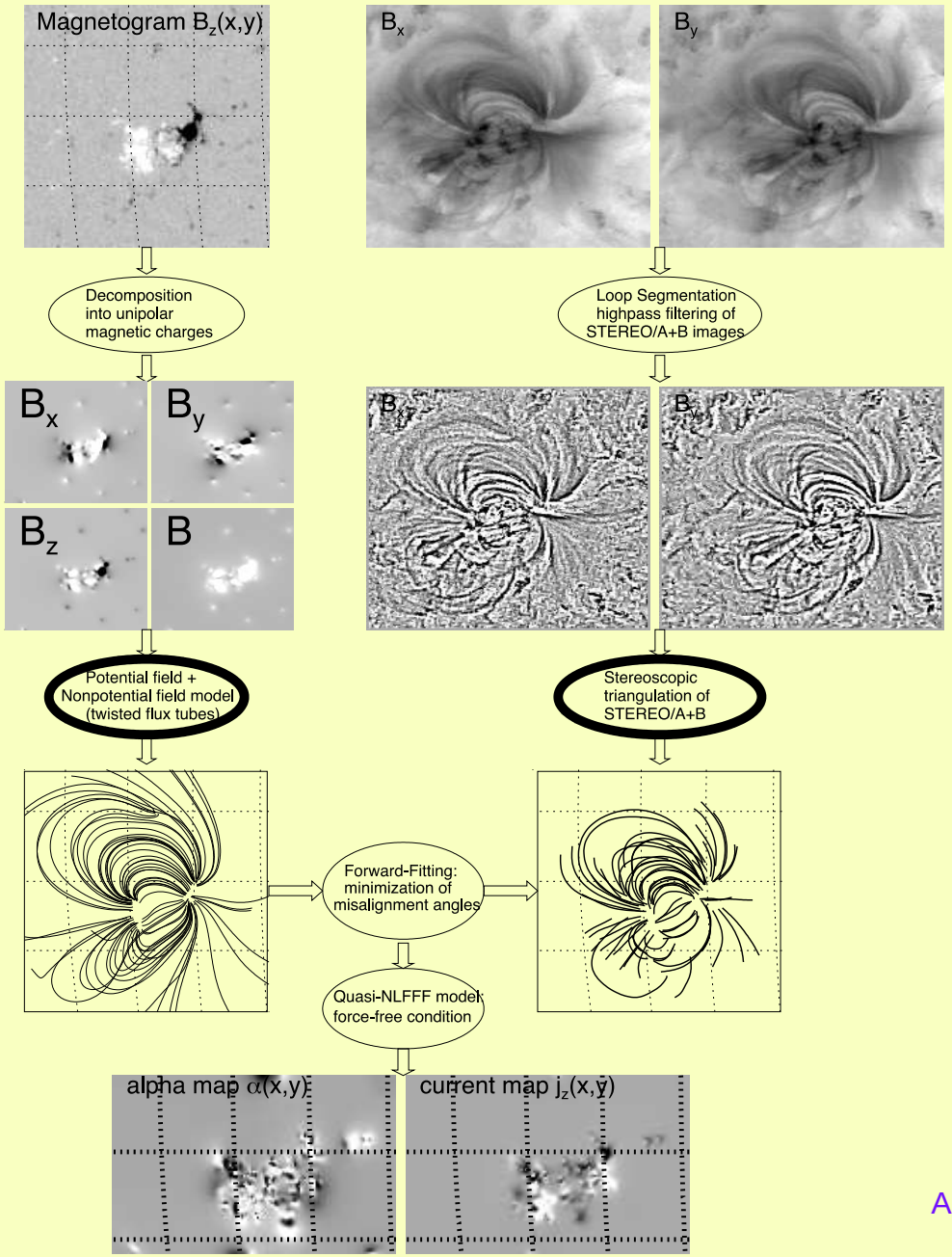


Aschwanden et al. (2012)

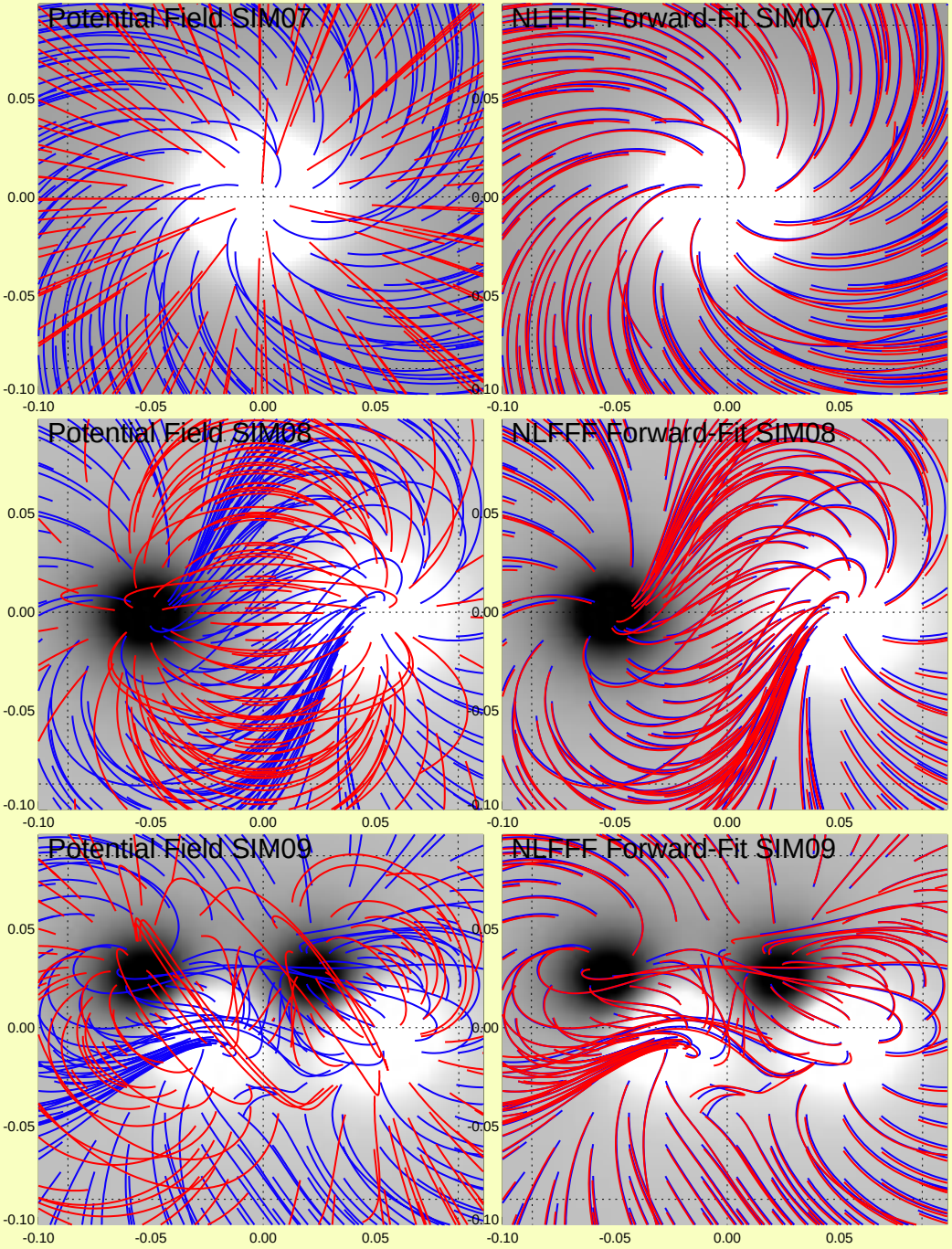


Analytical approximation of vertical-current model with buried magnetic charges

Difference between a potential field and a nonpotential field (with vertical twist)

Aschwanden (2013)
Solar Phys. 287, 369.

A 3D best-fit solution of the vertical-current NLFFF approximation fitted to traced coronal loops in AIA images.

20110215_011400, EVENT=12, FRAME= 0 / 13, RUN=run02

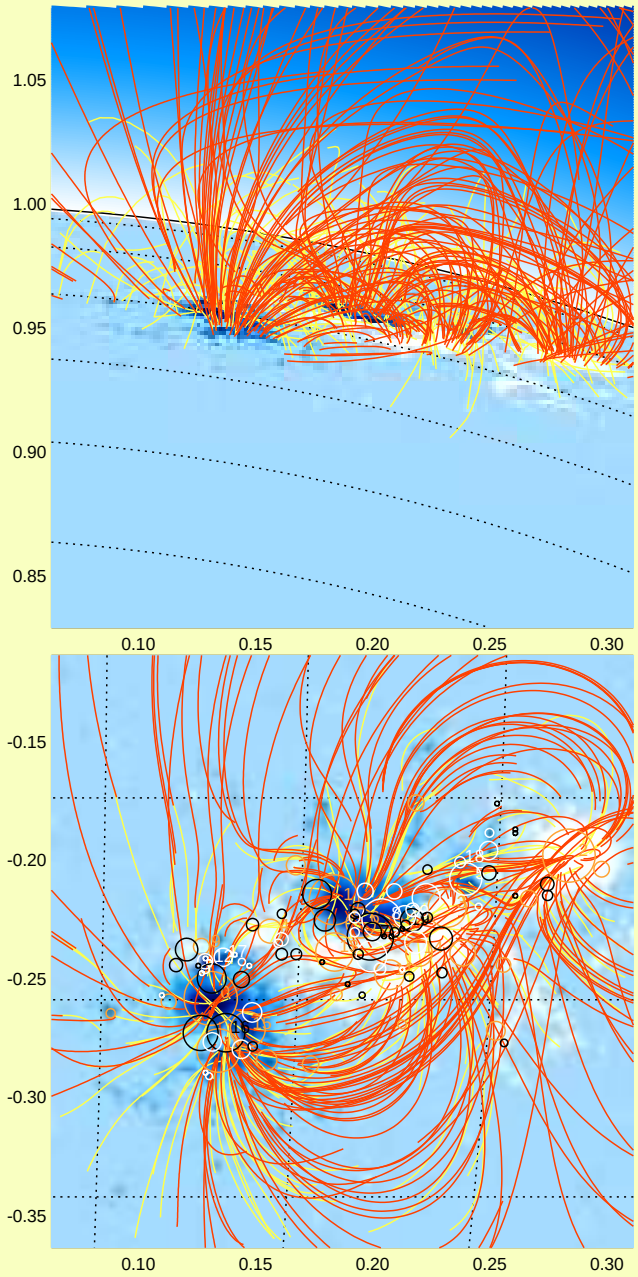


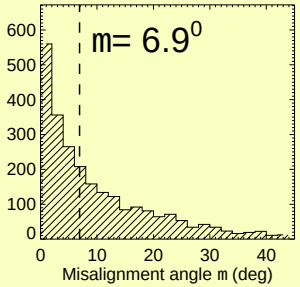


| | |
|---|---|
| NOAA | =11158 |
| Hel.pos. | =S21W12 |
| FOV | =0.25 |
| [x1,x2] | = 0.0628, 0.3128 |
| [y1,y2] | =-0.3635, -0.1135 |
| wave,nsm1, | = 6, 3 |
| thresh0,2,nsig | =0.0, 3.0, 3.0 |
| rmin,lmin,ngap | = 25, 25, 3 |
| ds,nh | =0.0020, 5 |
| dx_euv | = 0.000618 $R_{sun}$ |
| dx_mag | = 0.001500 $R_{sun}$ |
| nmag | = 100 / 100 |
| n_nlfff | = 25 |
| dfoot,dprox | = 0.015, 0.015 |
| nloopw,qripple | = 200, 0.50 |
| nall,ngood,nf | =497/298/285 |
| n1,n2,n3,n4,n5 | =11/0/0/188/0 |
| niter | = 25 / 73/100 |
| hmin,hmax | =0.001, 0.200 |
| nseg,mdim | = 9, 2 |
| nsmax | = 200 |
| da0 | = 1.0 |
| misalign | = 6.9 deg |
| div-free | = 4.5e-05 |
| force-free | = 1.1e-04 |
| weight curr | = 4.3e-01 |
| qB_rebin | = 1.017 |
| qB_model | = 1.091 |
| qiso_corr | = 2.467 |
| E_P | = 917.1 x $10^{30}$ erg |
| E_free | = 120.1 x $10^{30}$ erg |
| E_NP/E_P | = 1.131 |
| CPU | = 338.7 s |

--- loop tracings
--- field lines
o magn charges

Median 2D misalignment angle between NLFFF model and observed loops is 7 deg.

# Free Magnetic Energy

$$E_{\perp}^{free} = E_{N,\perp} - E_P = \frac{1}{8\pi}\left(\int B_{N,\perp}^2(\mathbf{x})dV - \int B_P^2(\mathbf{x})dV\right)$$

nwave =6
MAGNETIC SOURCES:
dsmag =0.0015
nmag,nmagmax= 56 100
dfoot = 0.015
wfit,bmin= 5, 300 G

misalign= 3.9 deg
div-free= 5.1e-05
force-free= 1.0e-04
weight curr= 6.1e-01
B_rebin/B_full = 1.022
B_model/B_rebin= 0.953

qiso_corr= 2.467
E_NP = 699.8 x $10^{30}$ erg
E_P = 667.0 x $10^{30}$ erg
E_free = 32.8 x $10^{30}$ erg
E_NP/E_P = 1.049
CPU = 137.9 s

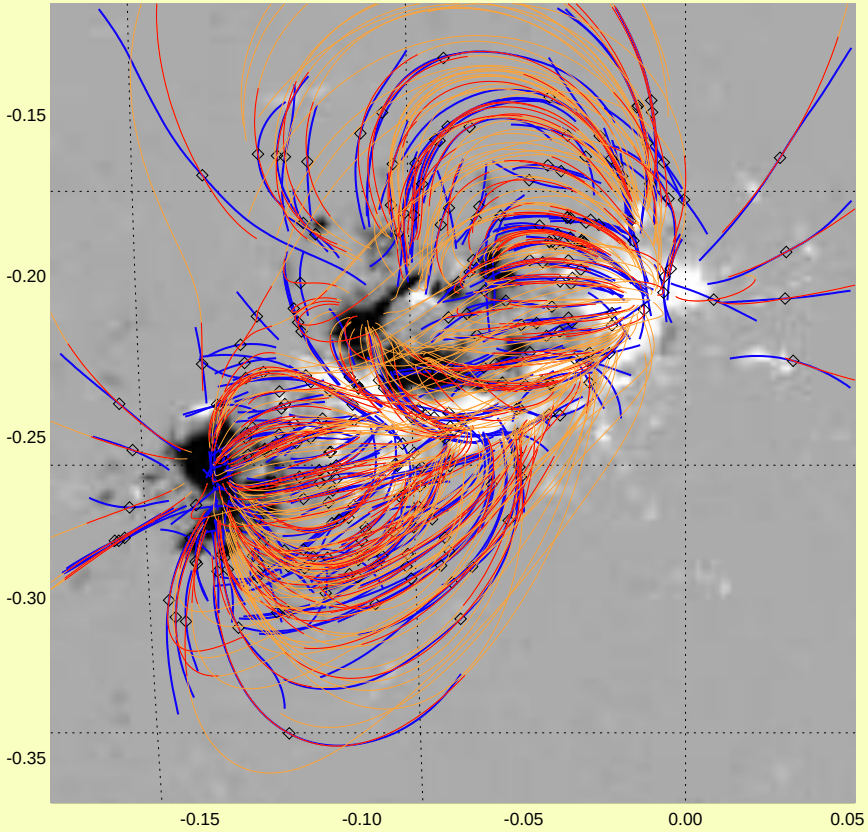


Decrease of free energy for event #10 (M6.6 flare): $dE_{flare}$=-(19±2) x $10^{32}$ erg

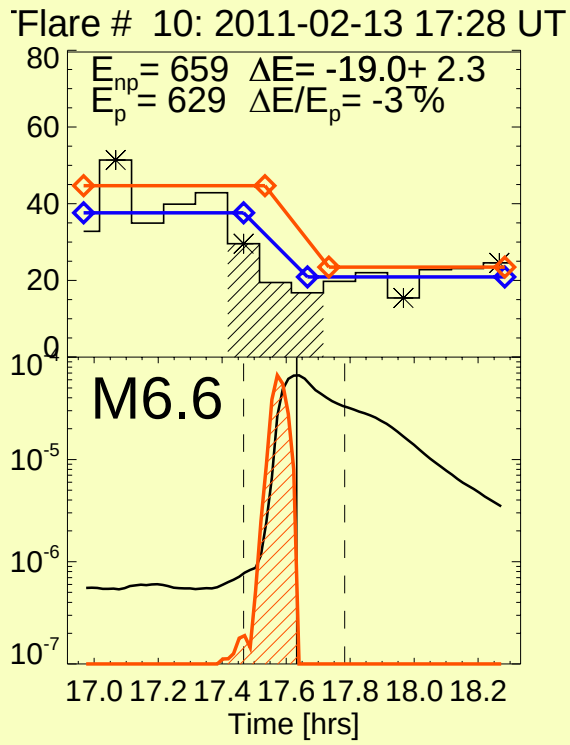

# Size Distributions of Magnetic Parameters

## Power law size distributions indicate self-organized criticality

Magnetic dissipated energy in flares: $E_{diss}$= $10^{30}$-$10^{33}$ erg

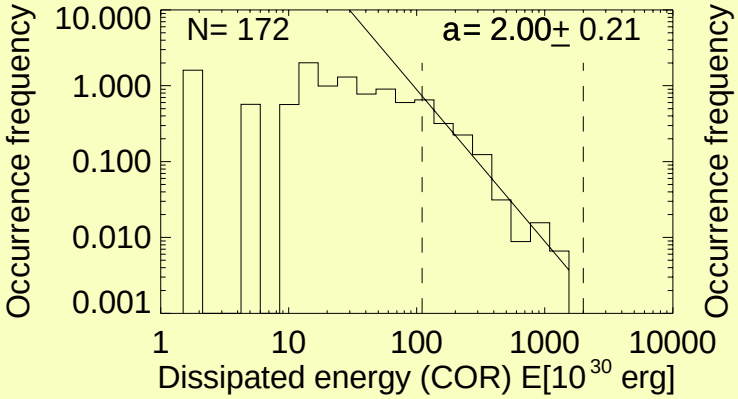


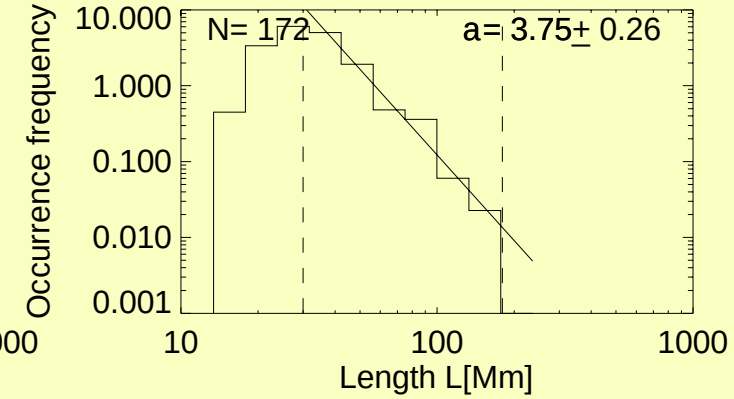


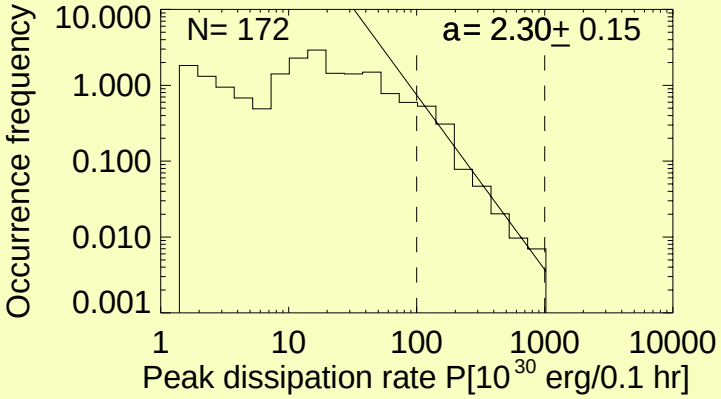


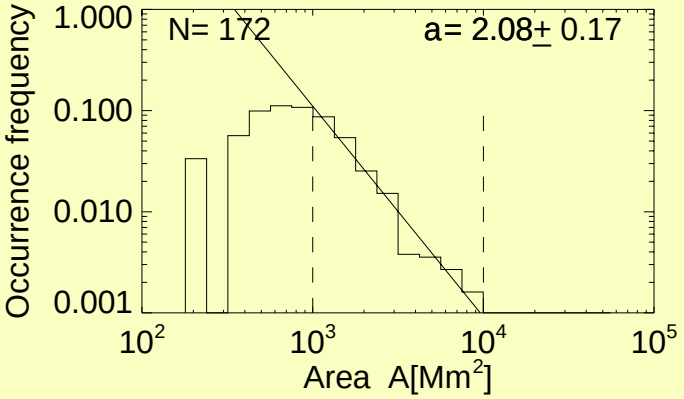


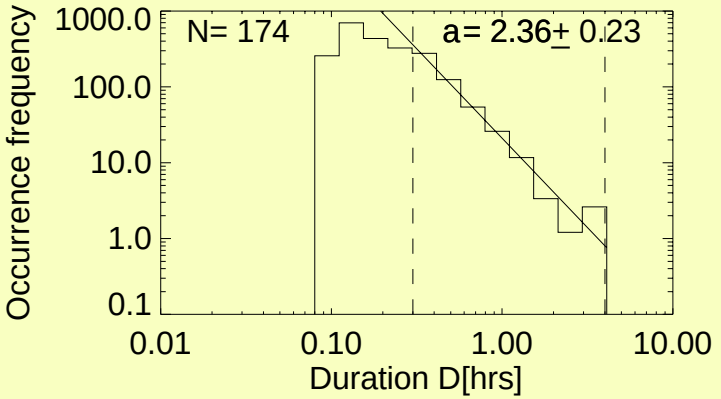


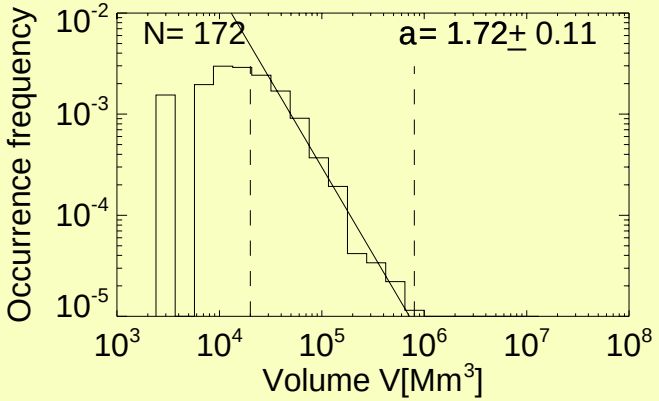

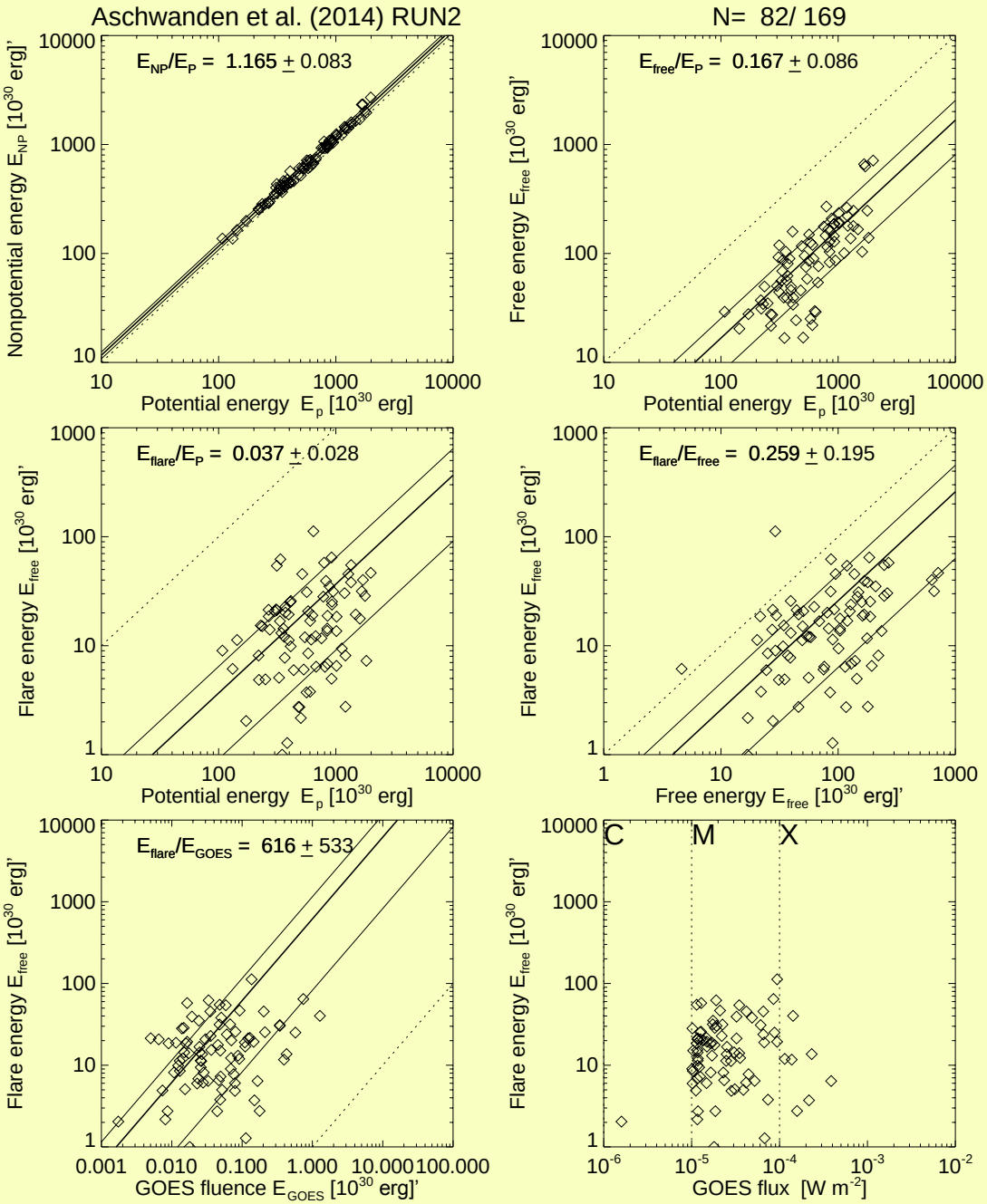


## Statistics :

82 of 169 (50 %) show a significant energy decrease during flares

49 of 169 (30%) show an apparent energy increase

34 of 169 (20%) show no significant changes

$E_{NP}/E_P = 1.16 \pm 0.08$

$E_{free}/E_P = 0.17 \pm 0.09$

$dE_{flare}/E_P = 0.04 \pm 0.03$

$dE_{flare}/E_{free} = 0.26 \pm 0.20$

$dE_{flare}/E_{GOES} = 600 \pm 500$

# Thermal Energetics

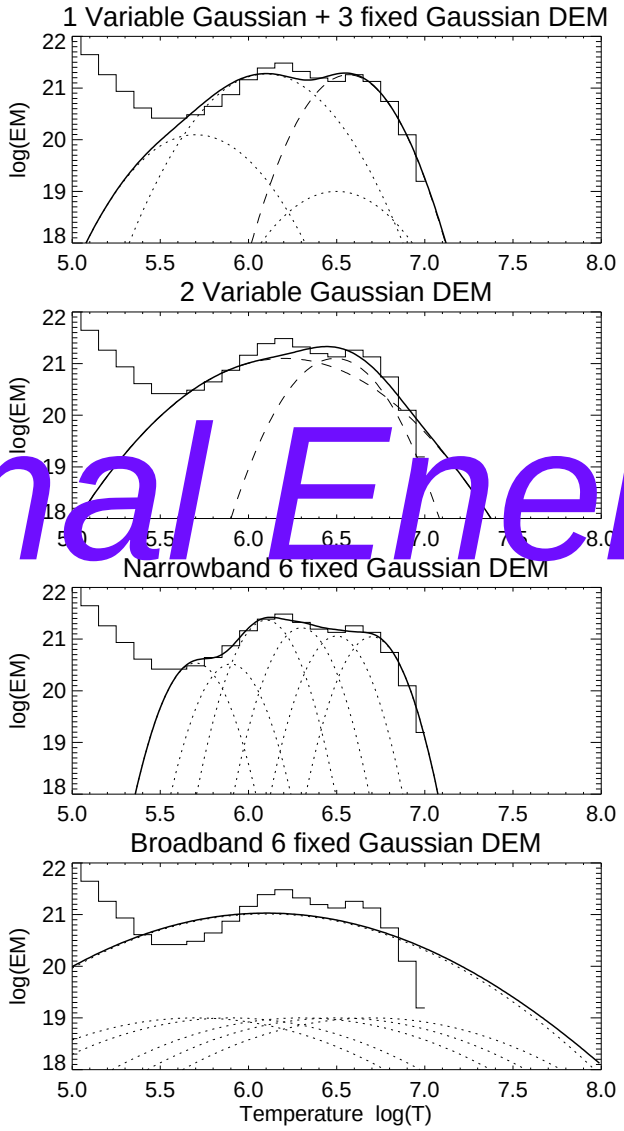

AIA + HMI / SDO

2011-Feb-14
20:35 UT

(5 hrs before
X2.2 flare)

FOV=0.3 $R_\odot$

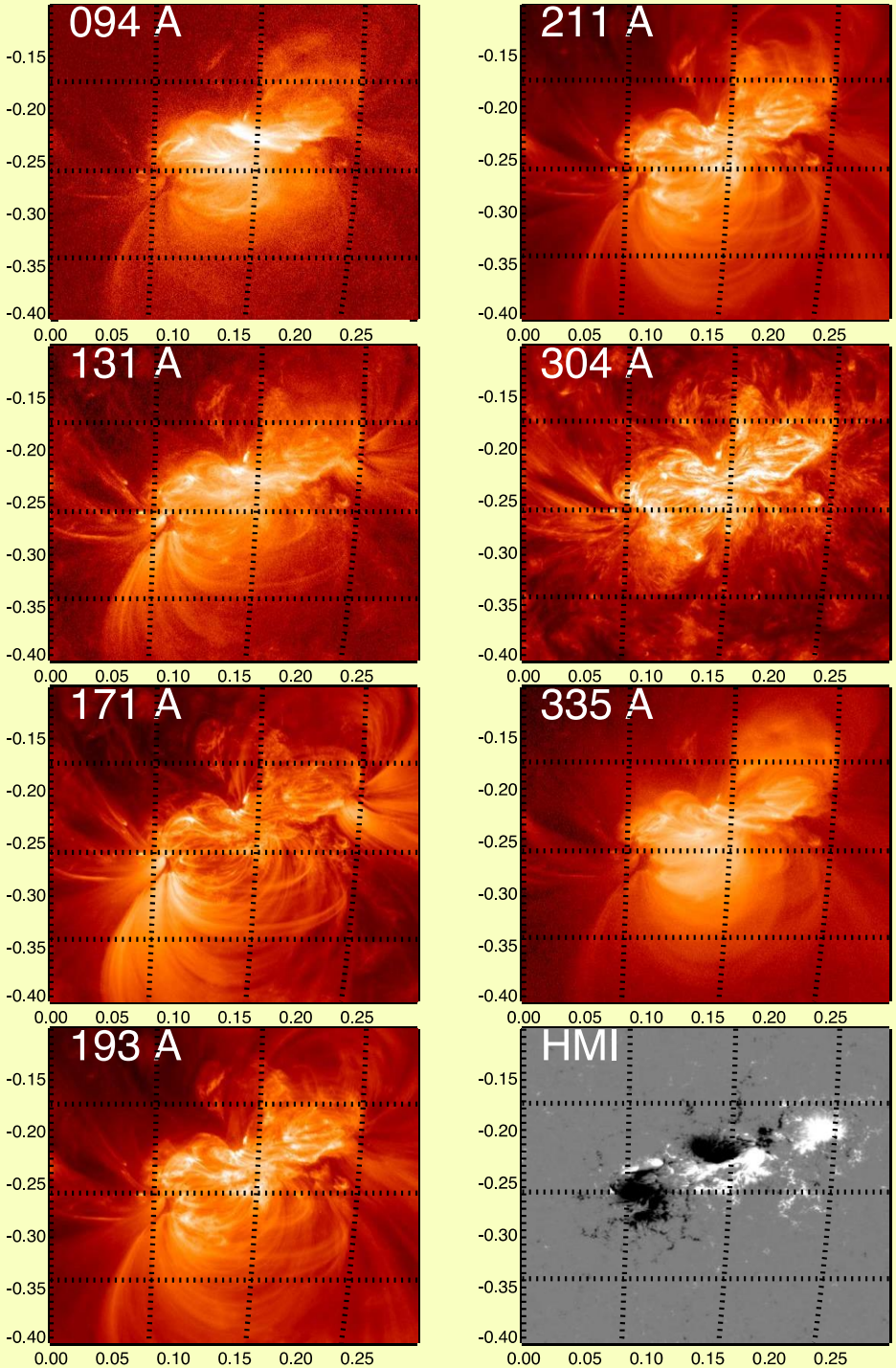


Aschwanden, Sun & Liu (2014)

# Nominal AIA Thermal Response Functions

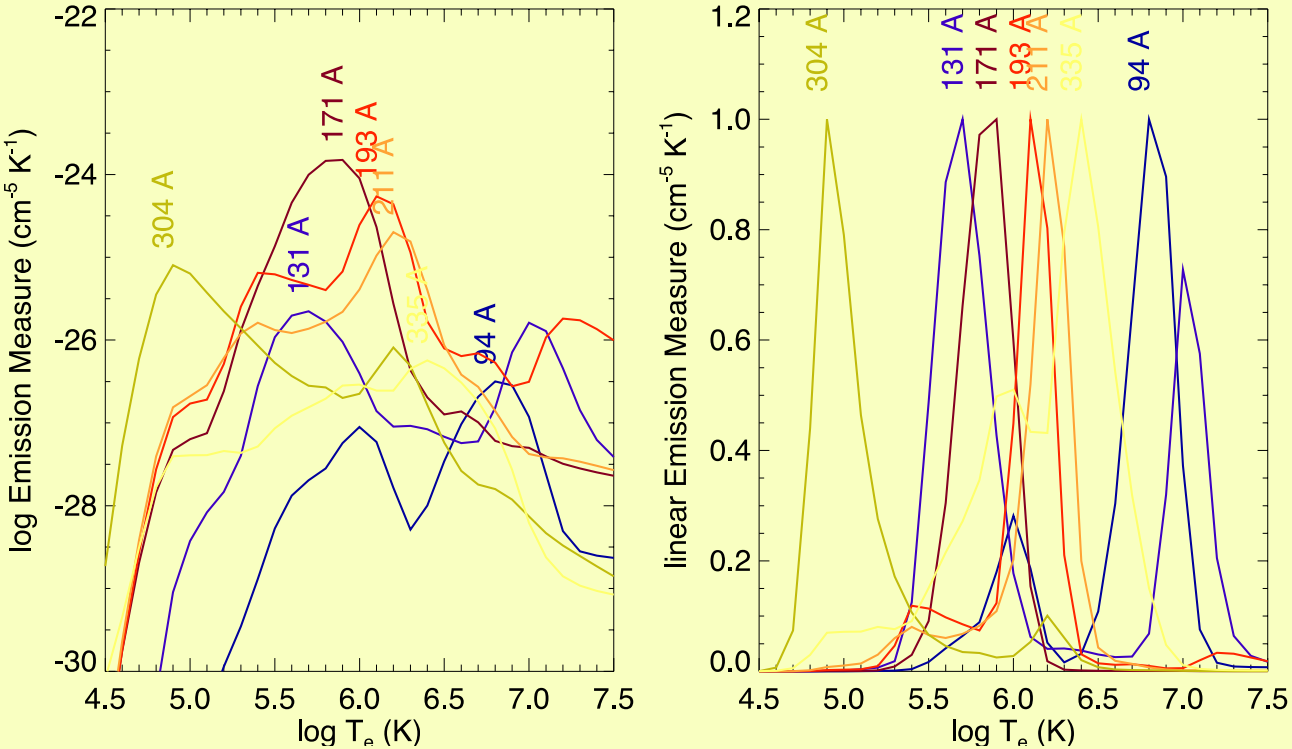


# Empirical AIA 94 A response function:

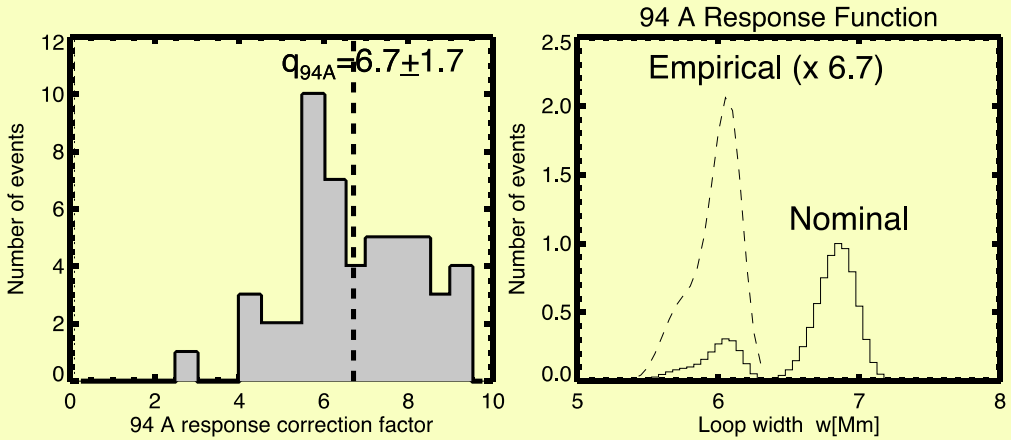

# Spatial Synthesis Gaussian DEM fits

$T_e$ peak

EM peak

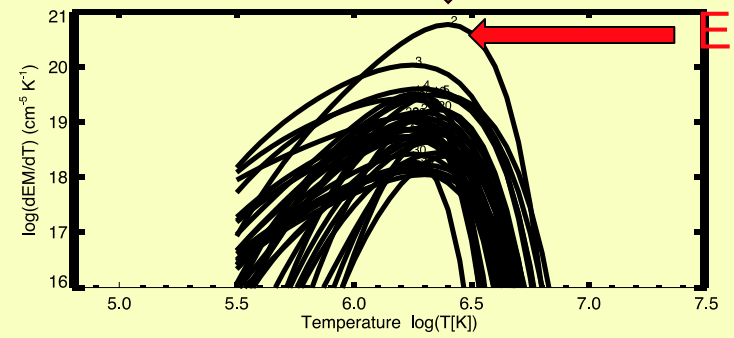


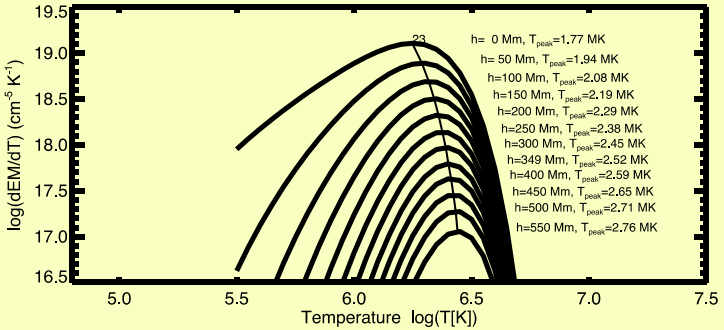


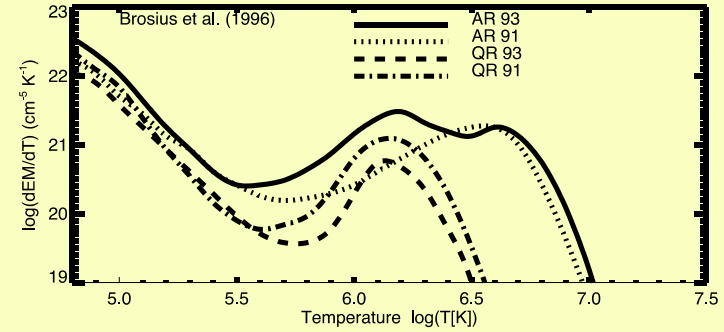


## 6 AIA filter fluxes:

$$F_\lambda(x,y) = \int \frac{dEM(T,x,y)}{dT} R_\lambda(T)\, dT \ ,$$

## Gaussian DEM distribution:

$$\frac{dEM(T,x,y)}{dT} = EM_p(x,y) \exp\left(-\frac{[\log(T) - \log(T_p(x,y))]^2}{2\sigma_T^2(x,y)}\right)$$

## Least-square fit:

$$\chi^2(x,y) = \frac{1}{(n-n_{free})} \sum_k \frac{[F^{obs}(x,y,\lambda_k) - F^{model}(x,y,\lambda_k)]^2}{\sigma_F^2(x,y,\lambda_k)} \ ,$$

## Flux uncertainty:

$$\sigma_F(x,y,\lambda_k) = \frac{1}{\Delta t_{exp} N_{bin}^2} \sqrt{\sum_i^{N_{bin}} \sum_j^{N_{bin}} F_\lambda(x_i,y_j) t_{exp}}$$

# Differential Emission Measure (DEM) Distributions
## spatially synthesized from single-Gaussians in each macropixel

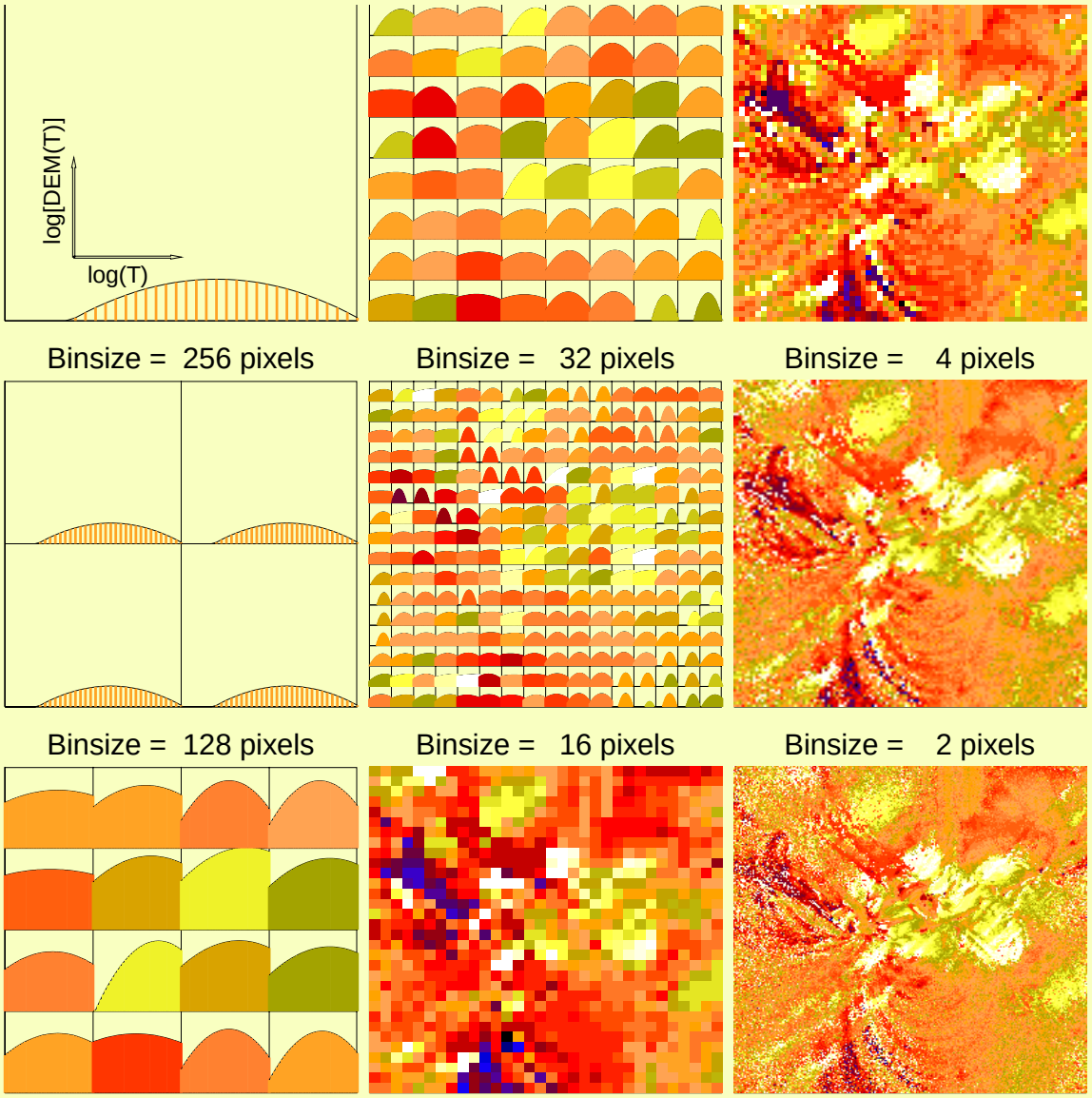


Aschwanden et al. (2015)

# Examples of Spatial-Synthesis DEMs during 12 Flares

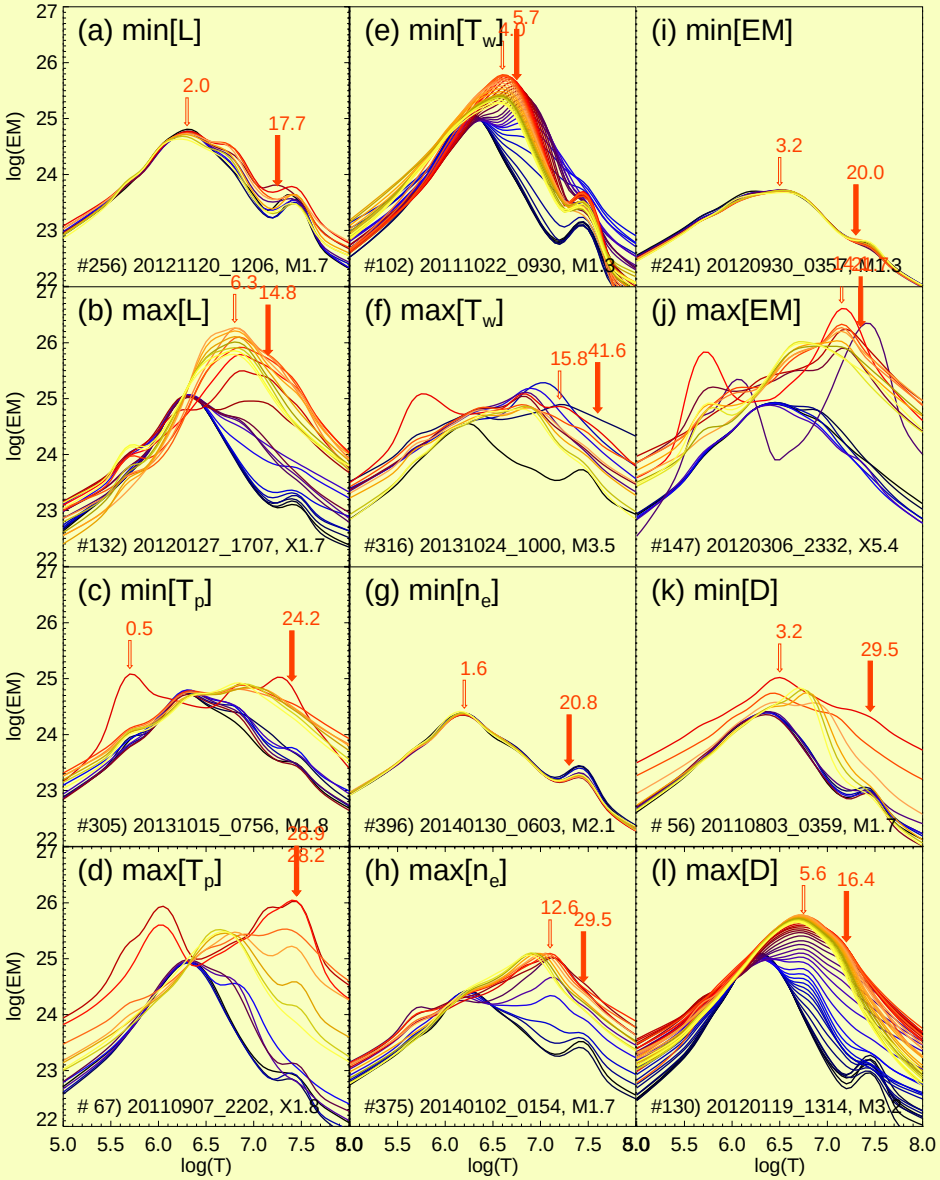


Peak T

EM-weighted T

# Size Distributions of Thermal Parameters

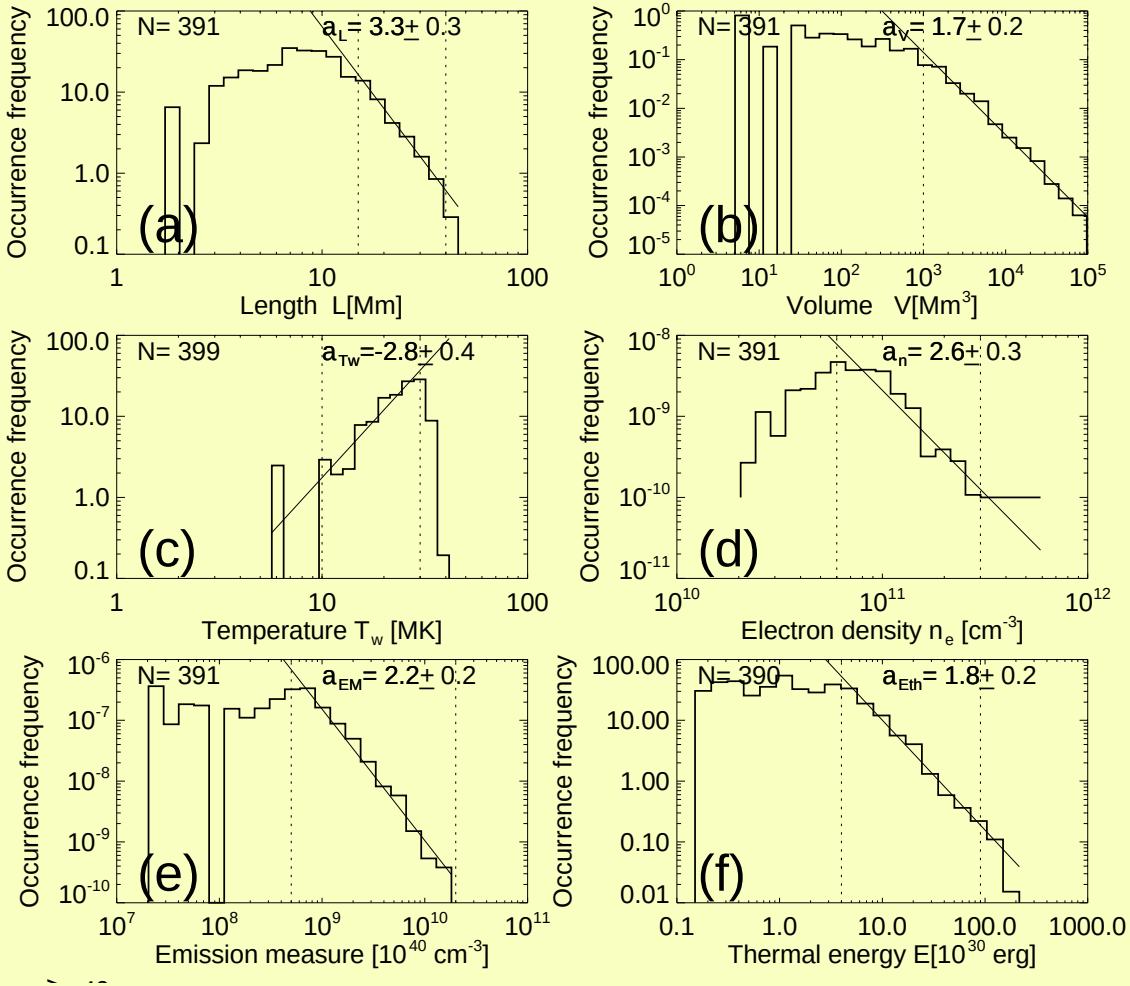


Power law distributions of N(L), N(V), N(EM) and N($E_{th}$) indicate self-organized criticality

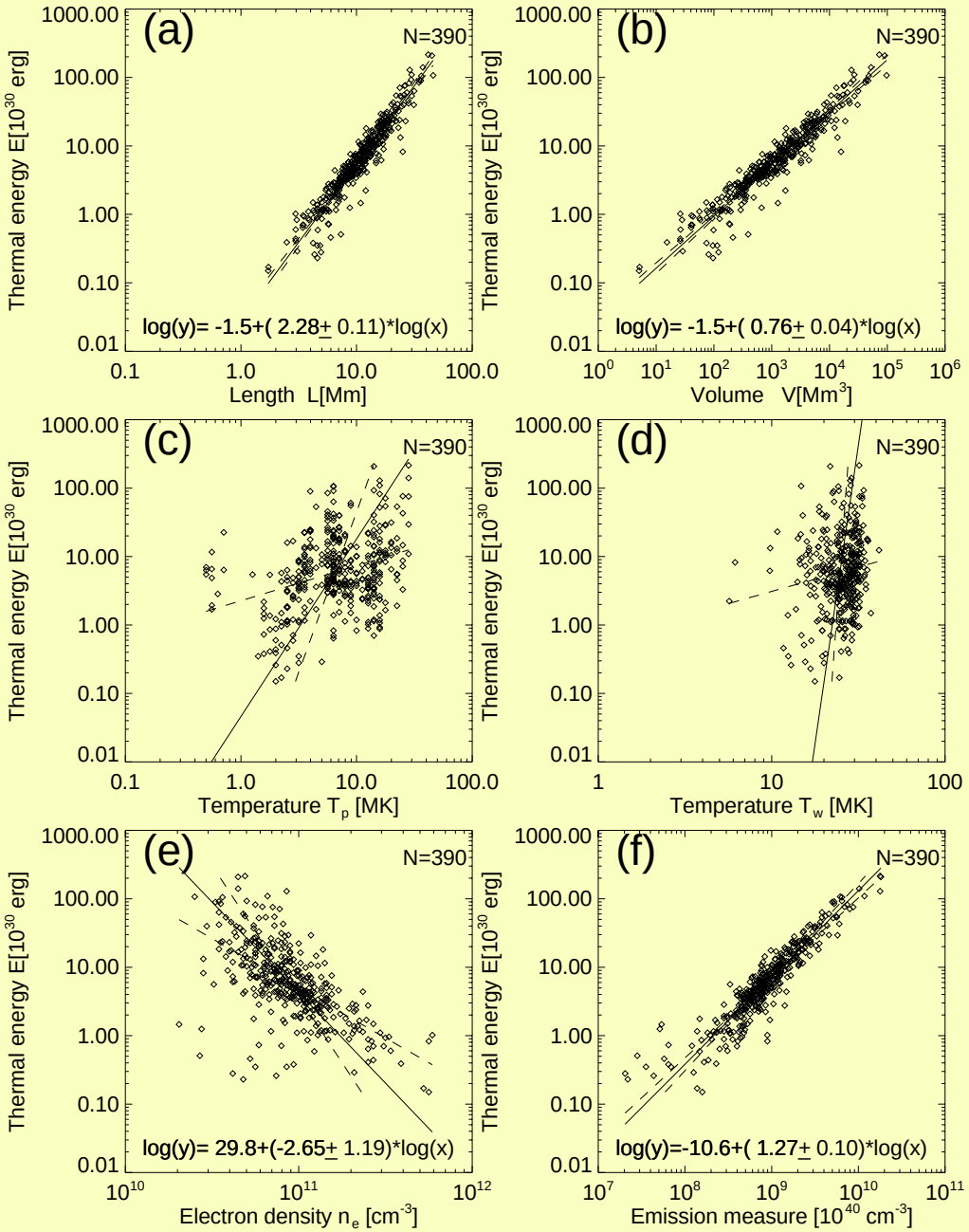


Multi-thermal Energy integrated over DEM(T)

Correlates with:

- length
- area
- volume
- emission measure

Small temperature range (M,X-class): (EM-weighted)

$T \sim 20\text{-}30$ MK

Reciprocal relationship to density:

$n_e \sim (EM/V)^{1/2}$

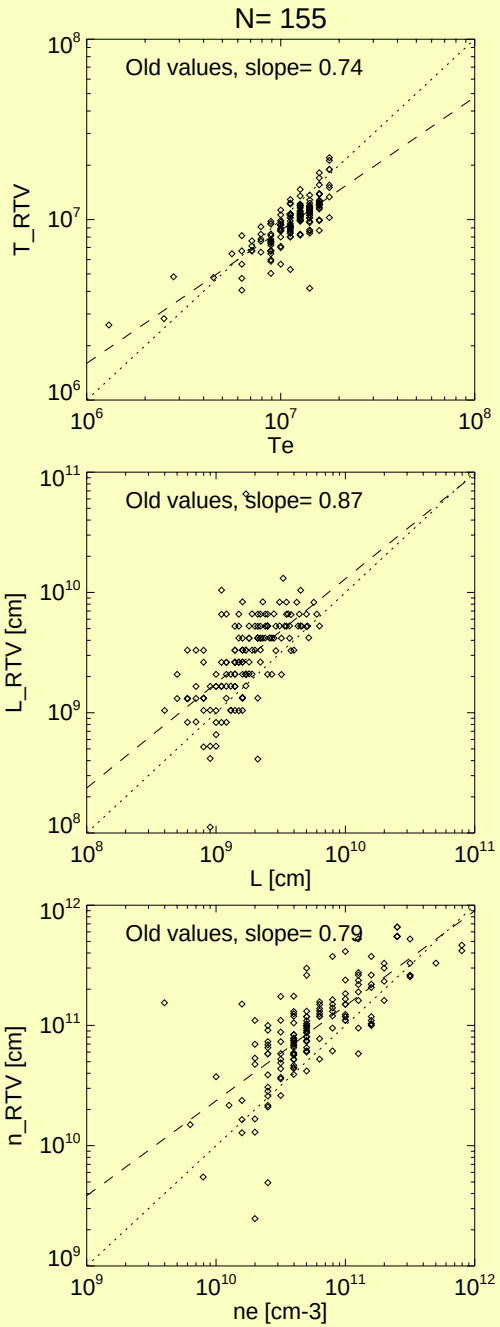


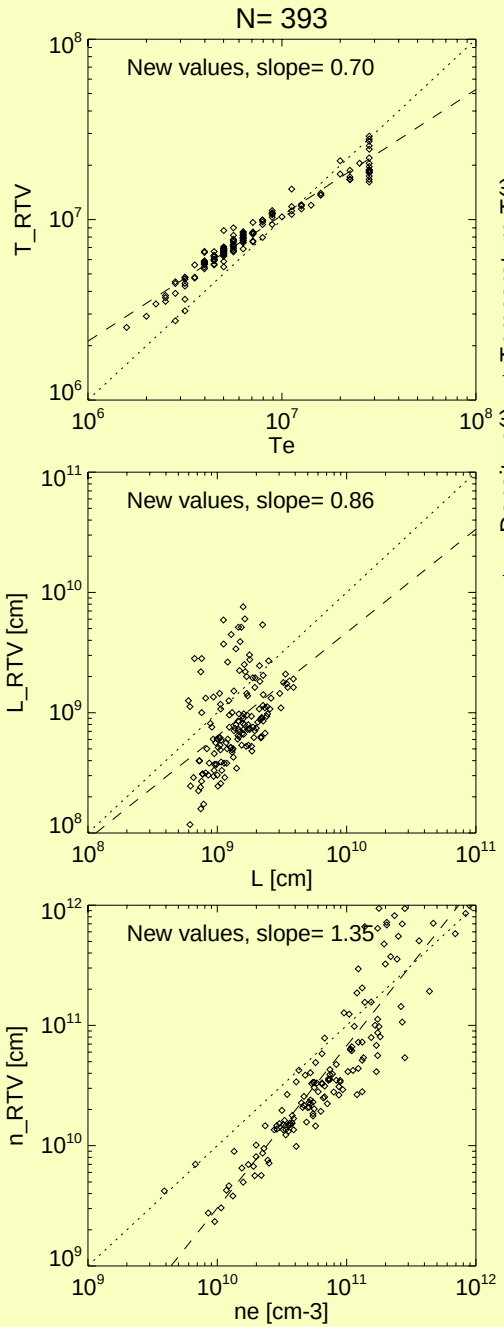


# RTV Scaling Laws

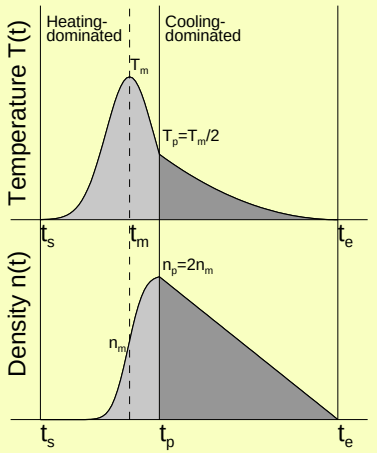


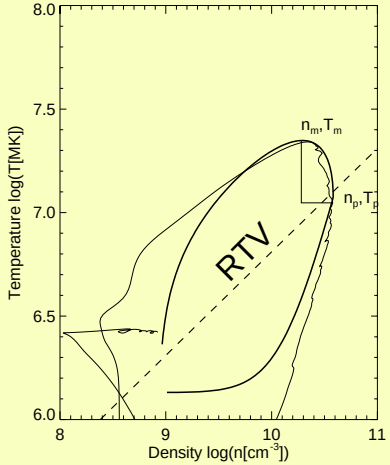


The RTV law can be applied to solar flares at the turnover point when heating rate equals the cooling rate, usually at peak of EM(t).

Here we test RTV scaling law with measured ($L$,$n_e$,$T_e$) hydrodynamic parameters from 393 SDO >M1.0 flares.

# RTV test of total emission measure (EM) and multi-thermal energy (Eth)

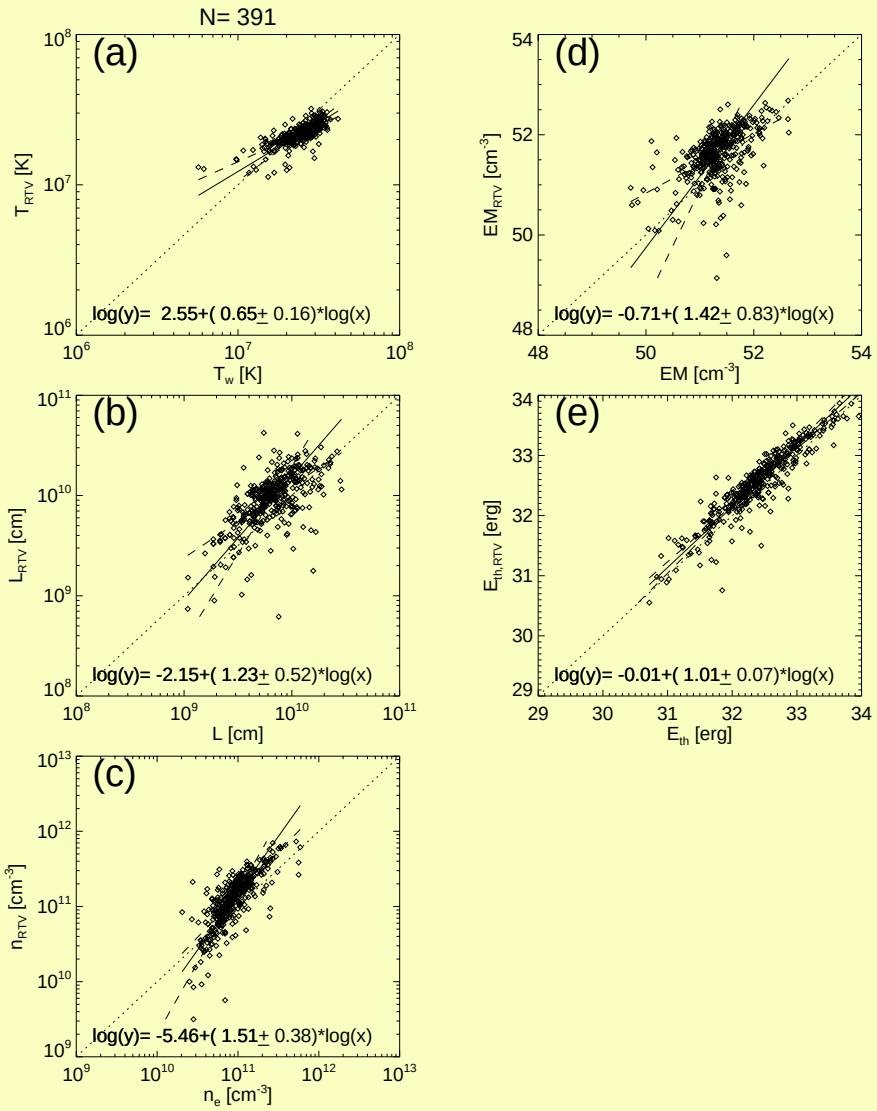


$$T_p = c_1\, n_p^{1/2}\, L_p^{1/2}\,, \quad c_1 = 1.1 \times 10^{-3}\,, \tag{13}$$

$$n_p = c_2\, T_p^2 L_p^{-1}\,, \quad c_2 = 8.4 \times 10^5, \tag{14}$$

$$L_p = c_3\, T_p^2 n_p^{-1}\,, \quad c_3 = 8.4 \times 10^5. \tag{15}$$

These are predicted three-parameter correlations that can be tested with our data. Another useful parameter is the total emission measure $\mathrm{EM}_p$, defined by the integral over the flare volume $V$,

$$\mathrm{EM}_p = \int n_p^2 dV = n_p^2 V = n_p^2 \left(\frac{2\pi}{3} L_p^3\right) = c_4\, T_p^4 L_p\,, \quad c_4 = 1.48 \times 10^{12}. \tag{16}$$

Furthermore, we will also determine the distribution of thermal energies,

$$E_{\rm th} = 3 n_p k_B T_p V_p = c_5\, T_p^3 L_p^2\,, \quad c_5 = 7.3 \times 10^{-10}, \tag{17}$$

which can be expressed as a function of the peak temperature $T_p$ and length scale $L_p$ by substituting the RTV scaling law for the density $n_p$ (Equation (14)). In addition, we have the RTV heating rate scaling law,

$$H \approx c_6\, T_{\rm max}^{7/2} L_{\rm loop}^{-2} = c_6\, T_p^{7/2} L_p^{-2}\,, \quad c_6 = 0.95 \times 10^{-6}. \tag{18}$$

# Ratio of Multi-thermal Energy to Dissipated Magnetic energy

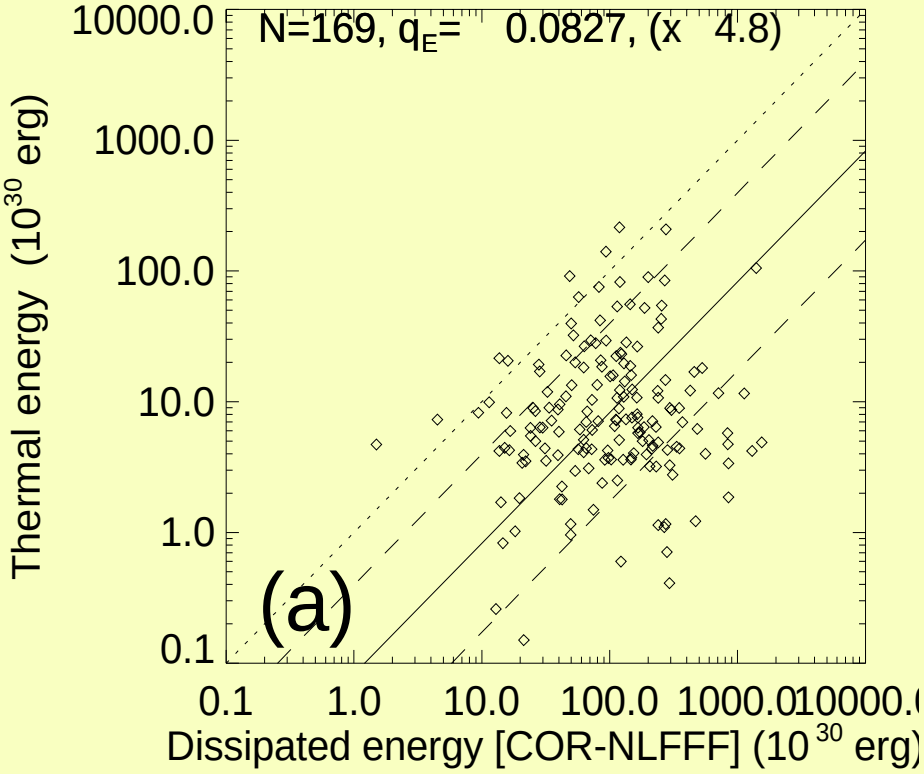


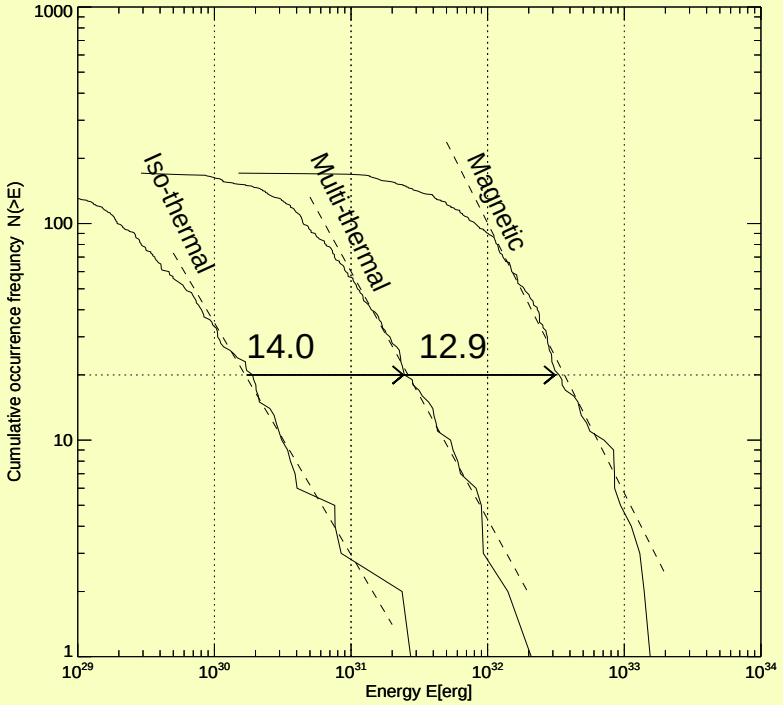


- The multi-thermal energy amounts to 8% of the magnetic energy (within a factor of 4.8, or a range of ~ 2%-40% )
- Magnetic (reconnection) processes are sufficient to produce the multi-thermal flare energy
- The iso-thermal energy underestimates multi-thermal energy by a factor of 14 (e.g., study of Emslie et al. 2012)

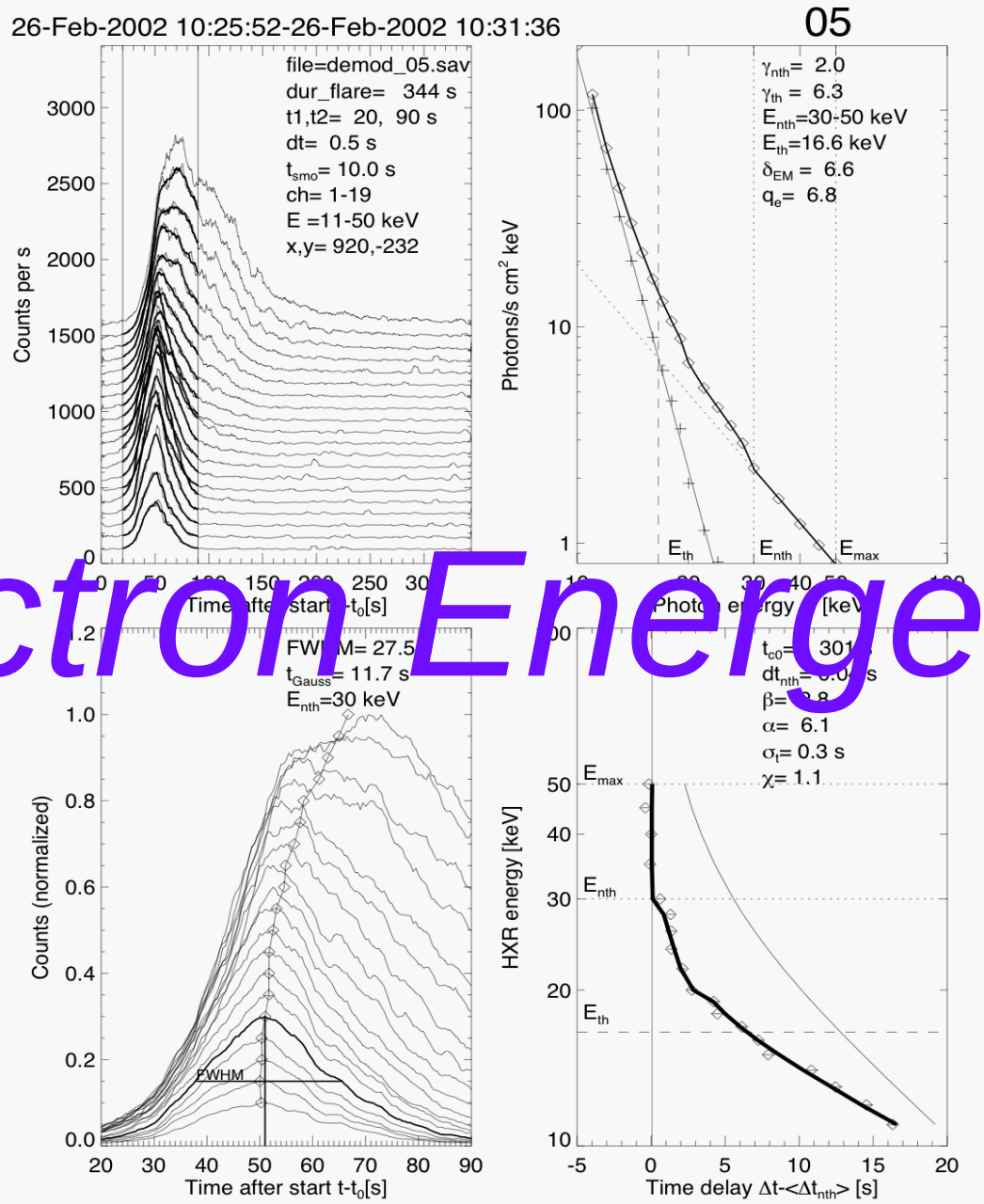


# Electron Energetics

## Nonthermal energy in electrons calculated from RHESSI:

- Fitting powerlaw to nonthermal photon spectrum
- Inverting electron injection spectrum (bremsstrahlung cross-section)
- Integration of electron energy spectrum E>20 keV

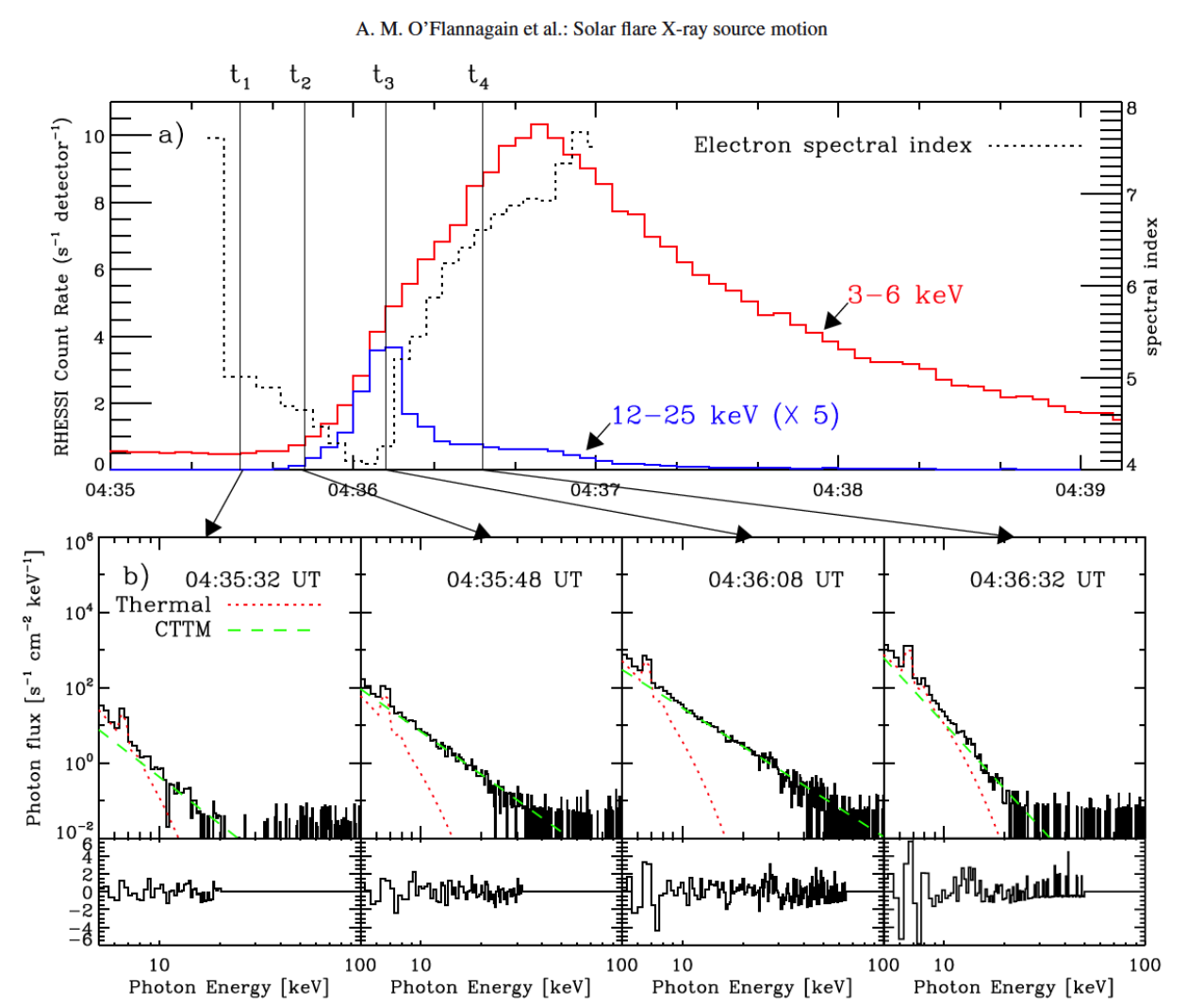


O'Flannagain Et al. (2013)

# The thick-target model with the warm-target low energy cutoff

Nonthermal spectum according to thick-target bremsstrhalung model (Brown 1971):

$$I(\varepsilon) = A\ \varepsilon^{-\gamma} \qquad (\text{photons cm}^{-2}\ \text{s}^{-1}\ \text{keV}^{-1}) \tag{1}$$

Thick-target (non-thermal) electron injection spectrum $f_e(e)$:

$$f_e(e) = 2.68 \times 10^{33}\ b(\gamma) A e^{-(\gamma+1)} \qquad (\text{electrons keV}^{-1}\ \text{s}^{-1})\ , \tag{2}$$

Total power in nonthermal electrons above a cutoff energy $e_c$:

$$P(e \geq e_c) = 4.3 \times 10^{24}\ \frac{b(\gamma)}{(\gamma - 1)}\ A\ (e_c)^{-(\gamma-1)} \qquad (\text{erg s}^{-1})\ . \tag{3}$$

Total (time-integrated) nonthermal energy $E_{\rm nt}$ during a flare:

$$E_{\rm nt} = \int_{t_{\rm start}}^{t_{\rm end}} P(e > e_c(t), t)\ dt \qquad (\text{erg})\ . \tag{4}$$

The bremsstrahlung spectrum $I(\varepsilon)$ of a thermal plasma (Brown 1974; Dulk & Dennis 1982):

$$I(\varepsilon) = I_0 \int \frac{\exp\left(-\varepsilon/k_B T\right)}{T^{1/2}} \frac{dEM(T)}{dT}\ dT\ , \tag{5}$$

Differential emission measure:

$$\left(\frac{dEM(T)}{dT}\right) dT = n^2(T)\ dV\ . \tag{6}$$

Combined thermal-plus-nonthermal spectrum:

$$I(\varepsilon) = I_{\rm th}(\varepsilon) + I_{\rm nt}(\varepsilon) = I_0 \int \frac{\exp\left(-\varepsilon/k_B T\right)}{T^{1/2}} \frac{dEM(T)}{dT}\ dT\ +\ A\ \varepsilon^{-\gamma}\ . \tag{7}$$

Effective low-energy cutoff $e_c$ of the warm-target plasma (Kontar et al. 2015):

$$e_c \approx (\xi + 2)\ k_B T_e = \delta\ k_B T_e\ . \tag{8}$$

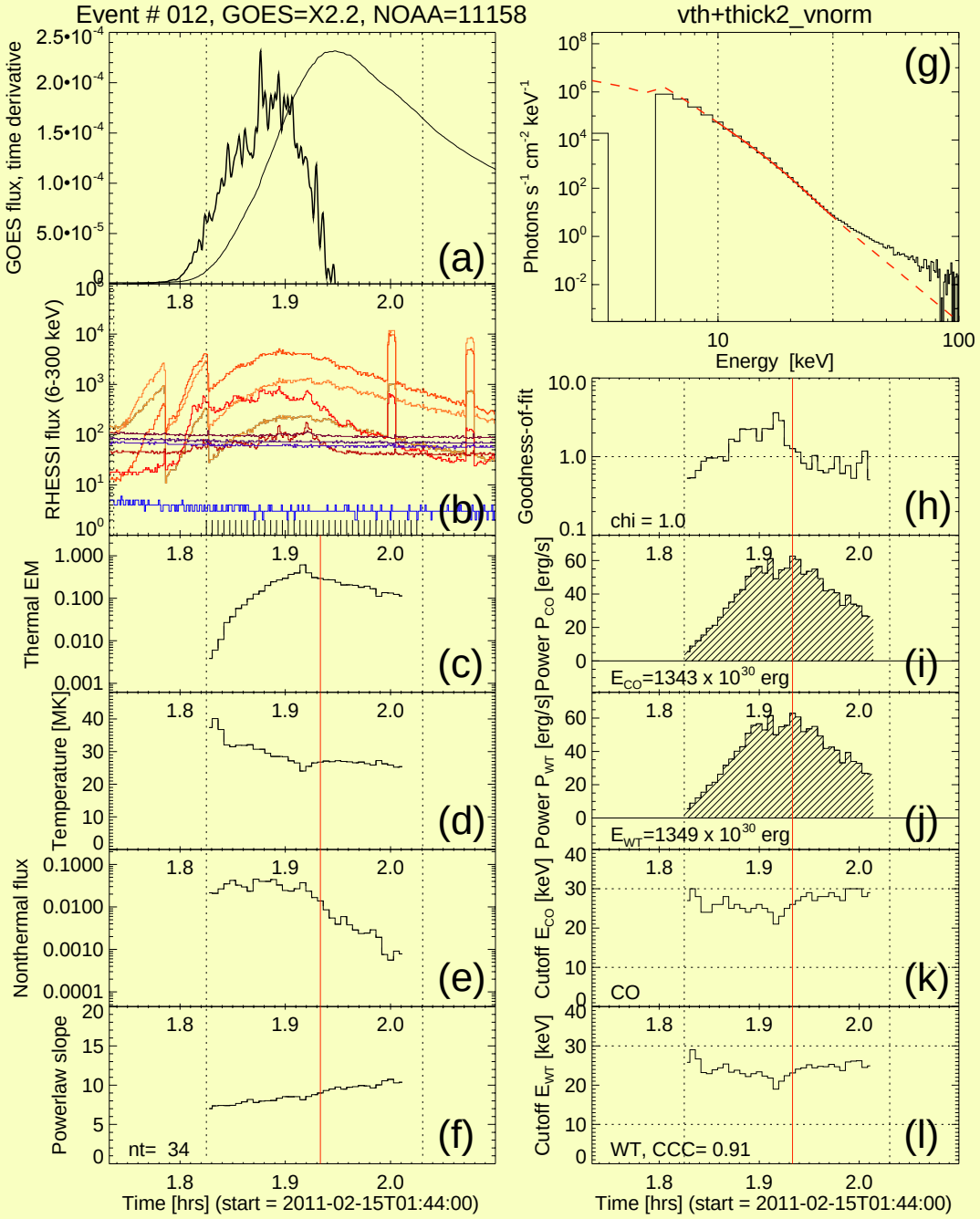


## Example of analyzed Flare (X2.2 GOES class

(a) GOES flux and time derivative
(b) RHESSI flux
(c) Thermal EM
(d) Electron temperature
(e) Non-thermal flux
(f) Non-thermal power law slope
(g) Spectral fit
(h) Goodness-of-fit
(i) Power (cross-over method)
(j) Power (warm-target method)
(k) Low energy cutoff (cross-over)
(l) Low energy cutoff (warm-target)

The low energy cutoffs correlate (CCC=0.91) between cross-over and warm-target method

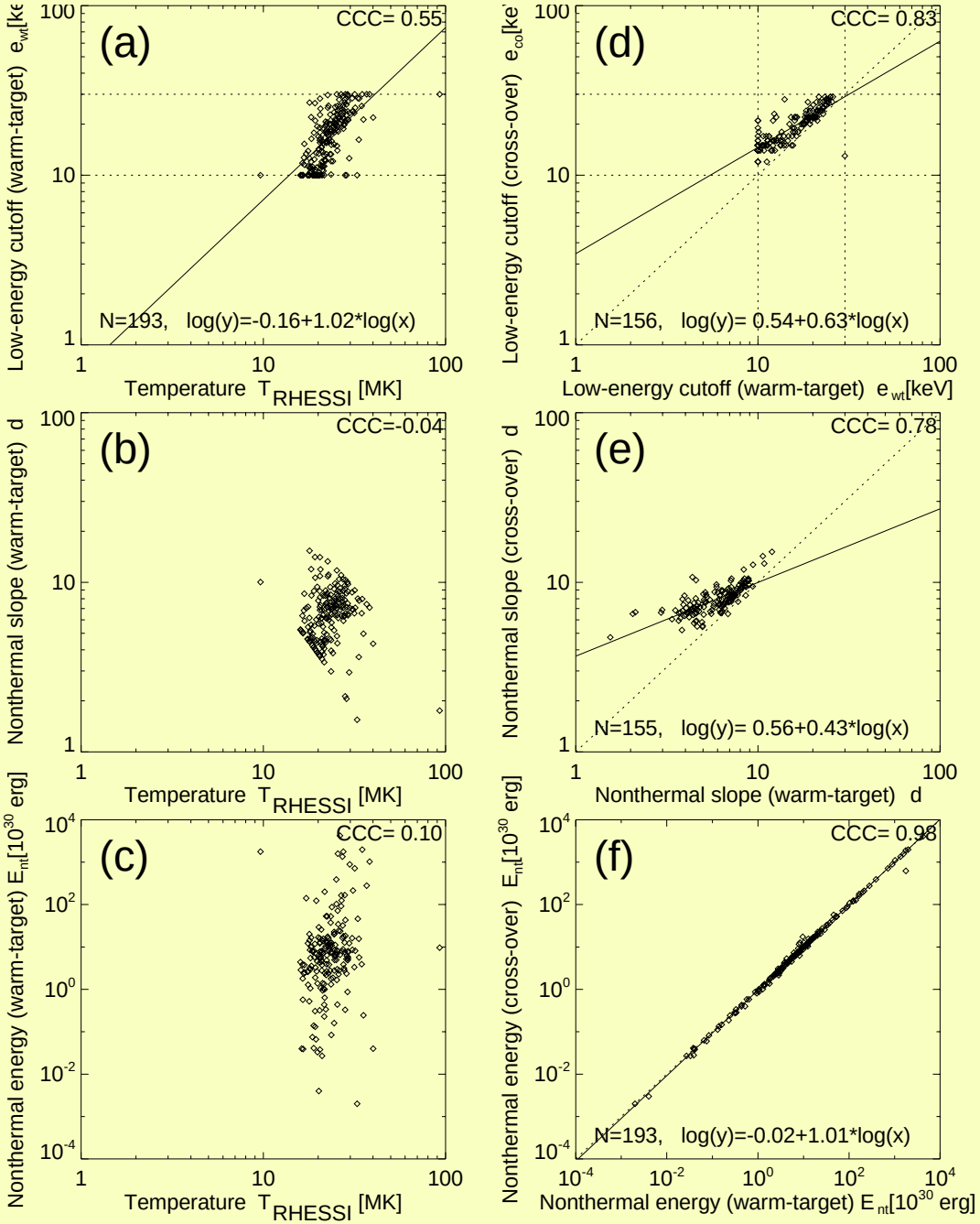


Low-energy cutoff is correlated with:

- temperature
- nonthermal slope

The nonthermal energy is highly correlated between the cross-over and warm-target method (CCC=0.98)

# Non-thermal energy vs. dissipated magnetic energy

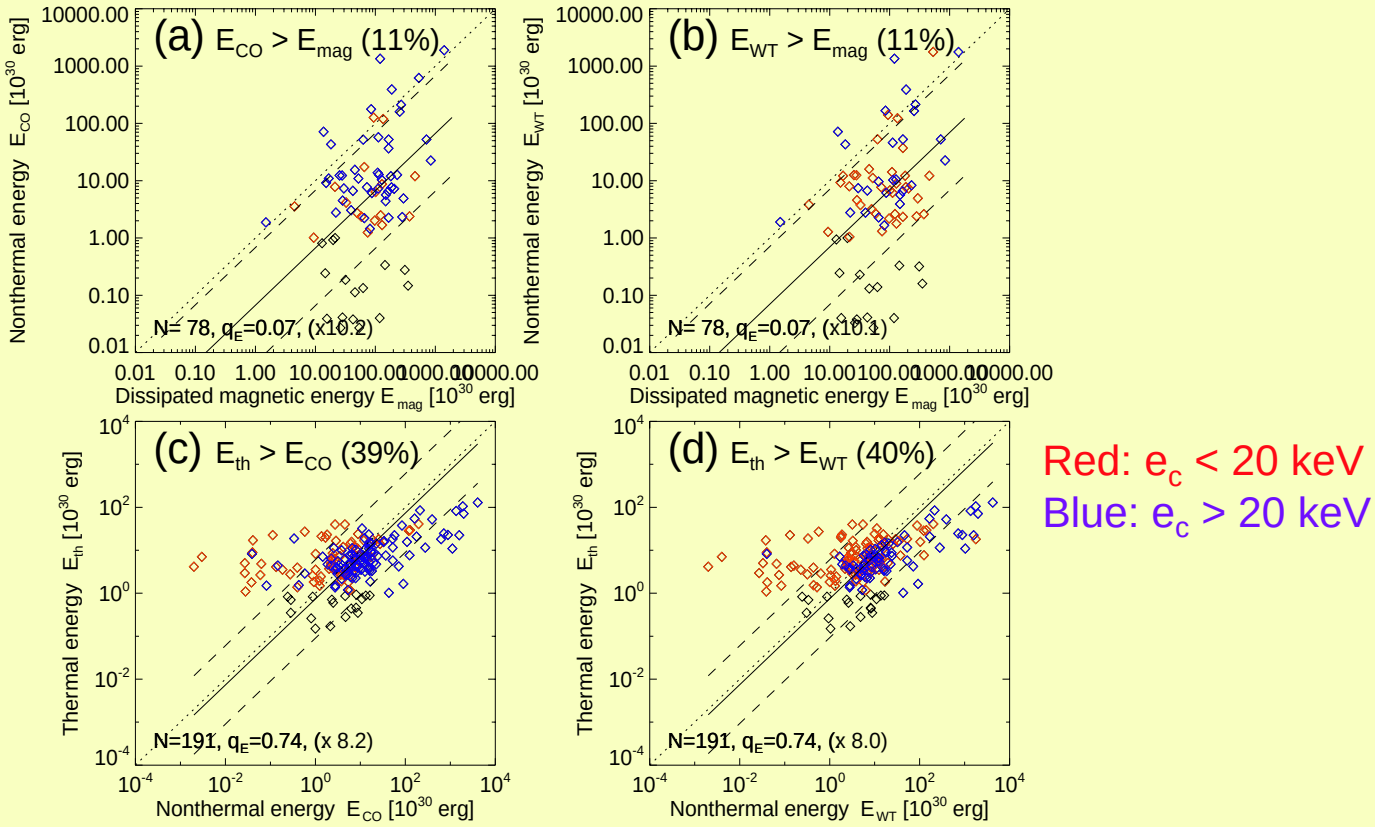


Red: $e_c$ < 20 keV
Blue: $e_c$ > 20 keV

- The non-thermal energy (in accelerated electrons) accounts in the logarithmic mean for 7% of the dissipated magnetic energy → Magnetic (reconnection) is sufficient to accelerate particles.

- The thermal energy exceeds the non-thermal energy in 40% → "Failure of the thick-target model", requires additional heating sources (thermal conduction fronts, direct heating processes).

Power law distributions of magnetic, nonthermal, and thermal energies.

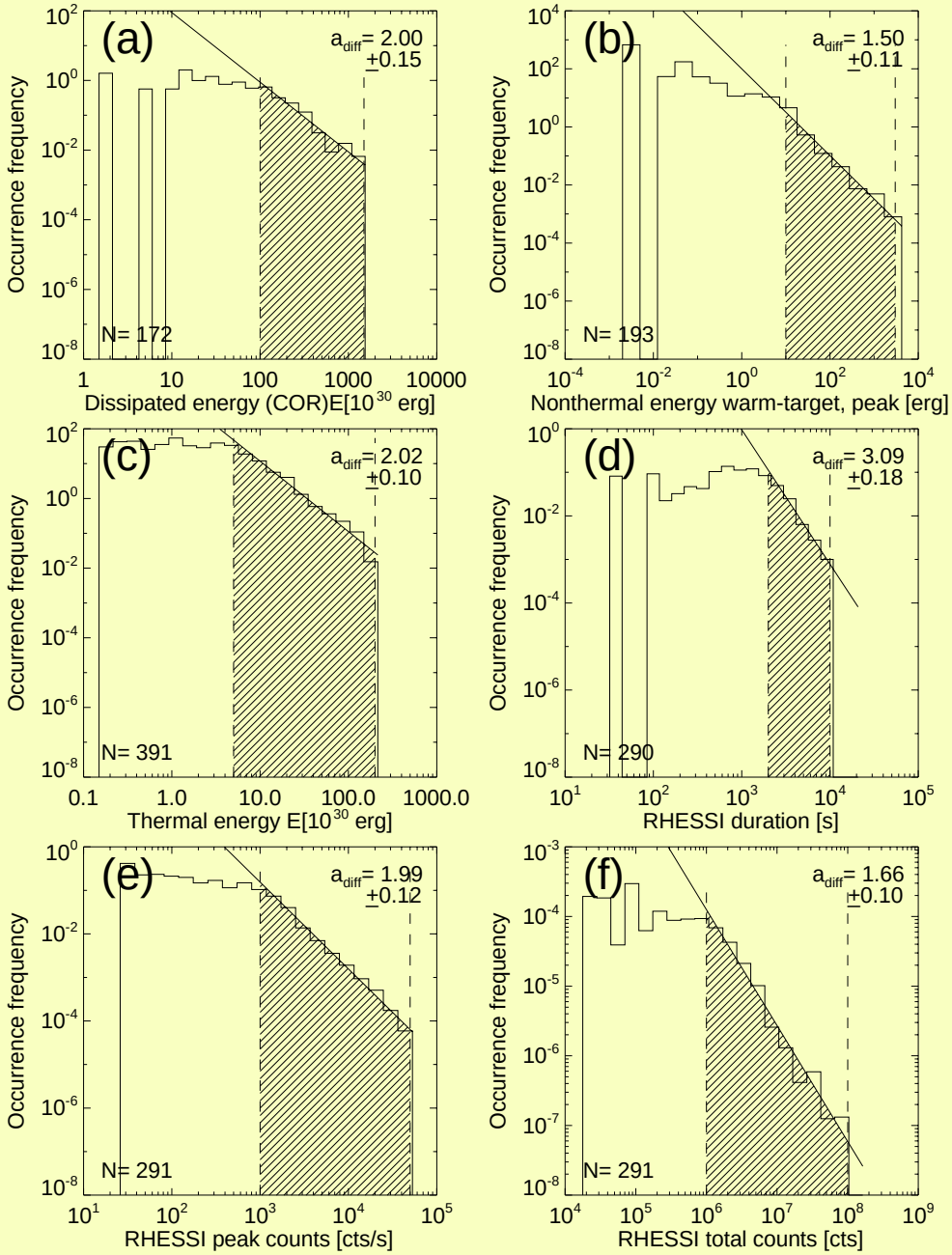

# Size distributions for magnetic, thermal, nonthermal energies

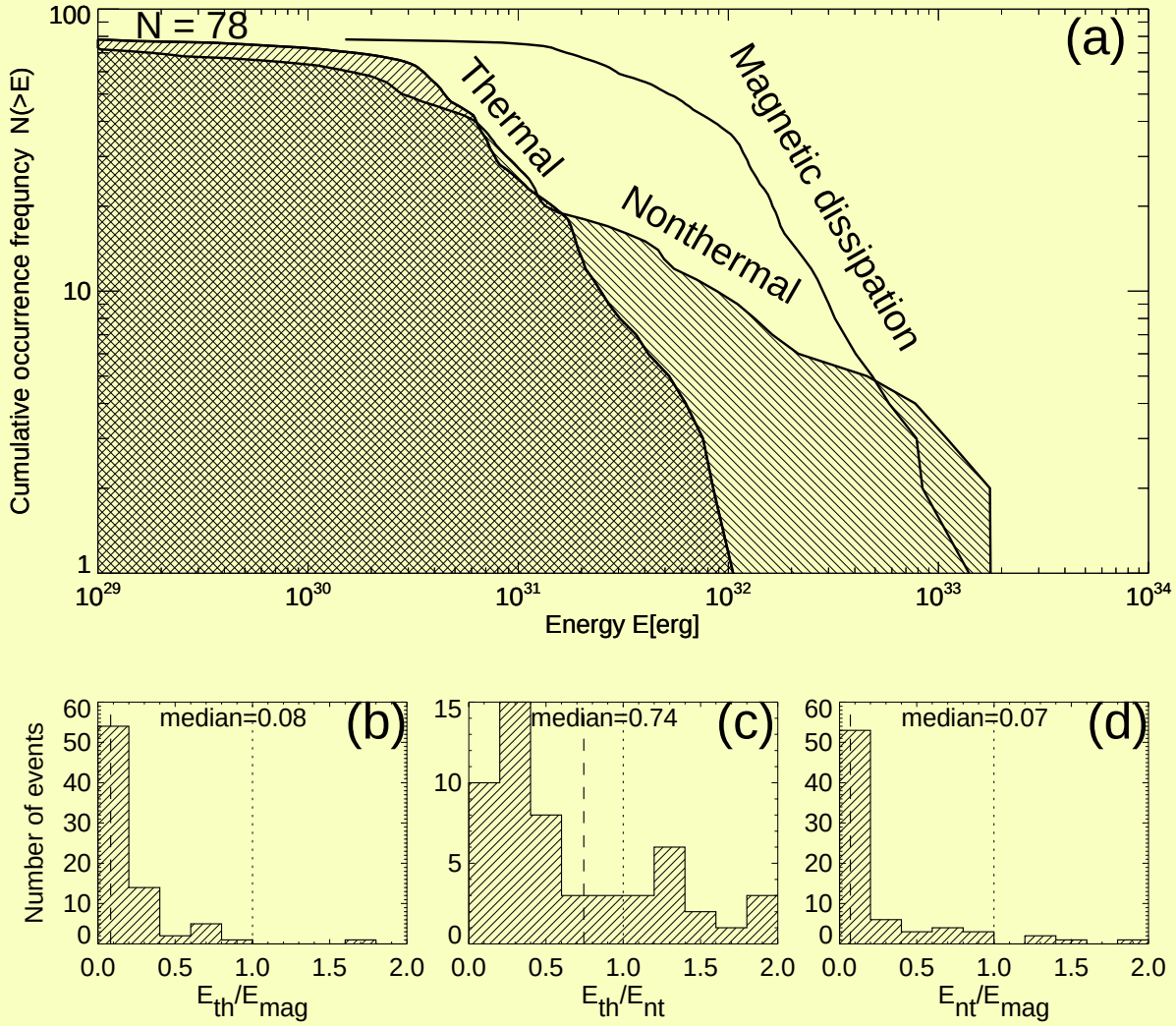


The ratio of nonthermal to dissipated magnetic energies varies systematically with the flare magnitude.

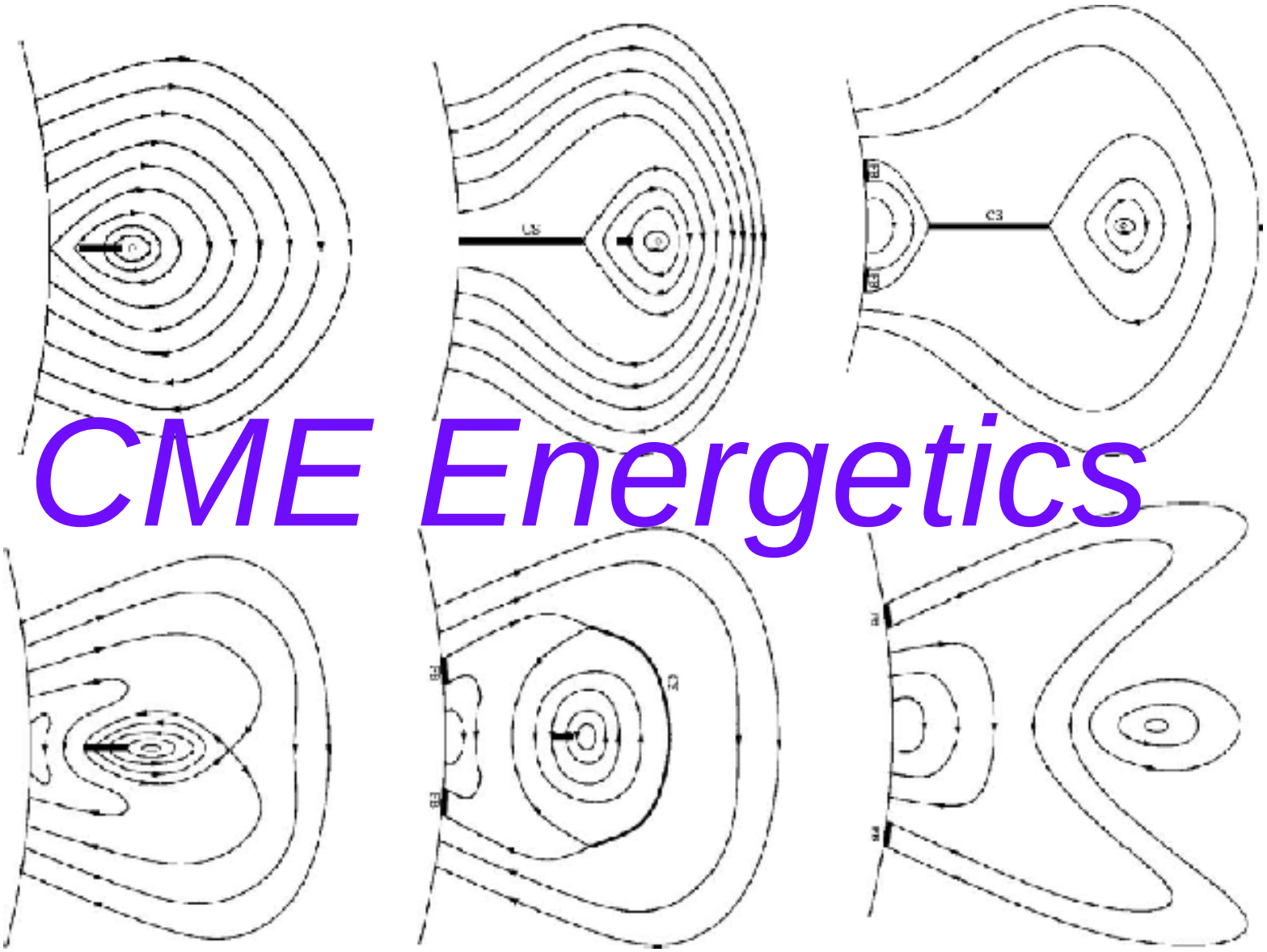

# CME Energetics

# CME Mass Determination from White Light Coronagraphs

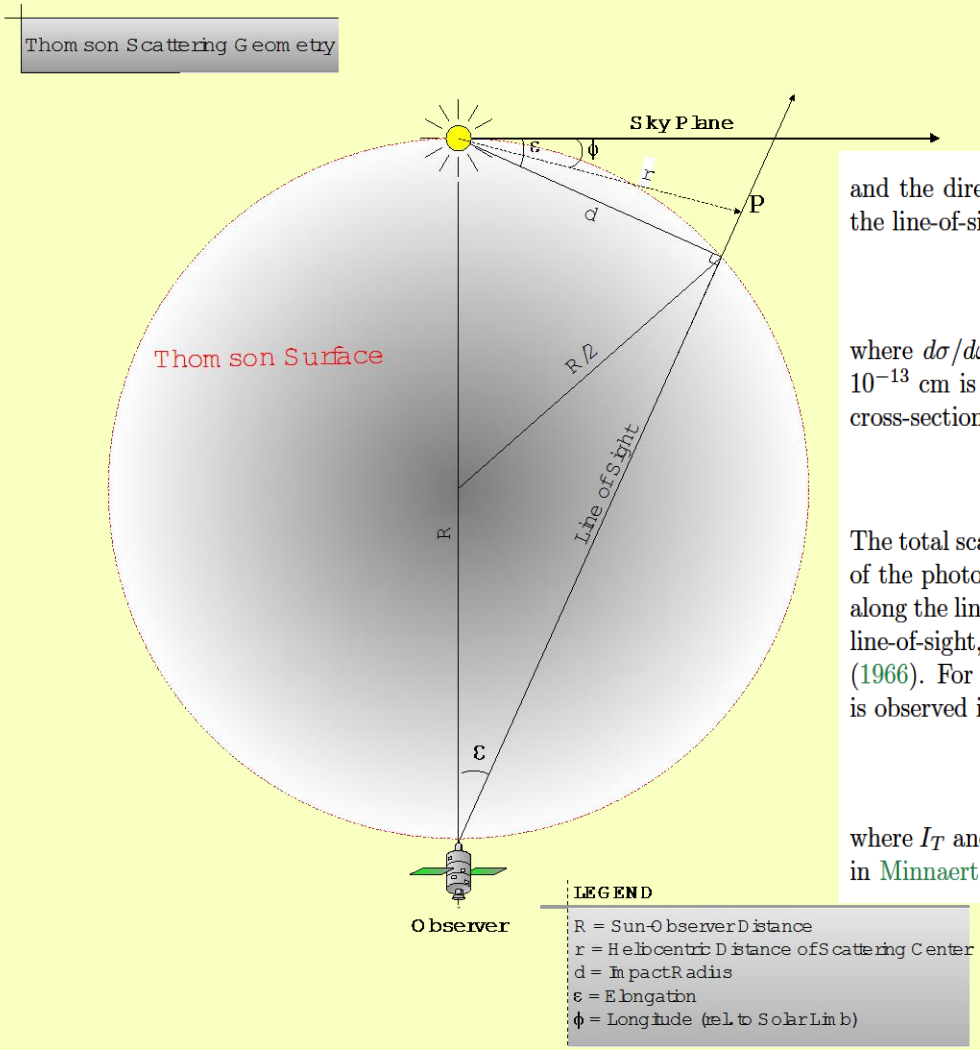


and the direction to the observer. The scattering cross-section depends on the angle $\chi$ between the line-of-sight and the radial direction through the scattering electron as (Jackson, 1962),

$$\frac{d\sigma}{d\omega} = \frac{1}{2} r_e^2 (1 + \cos^2 \chi) \,, \tag{8}$$

where $d\sigma/d\omega$ is the differential cross-section in units of $[\,\mathrm{cm}^2\ \mathrm{sr}^{-1}]$ and $r_e = e^2/m_e c^2 = 2.82 \times 10^{-13}$ cm is the classical electron radius. By integrating over all solid angles we obtain the total cross-section for perpendicular scattering, the so-called *Thompson cross-section* for electrons,

$$\sigma_T = \frac{8\pi}{3} r_e^2 = 6.65 \times 10^{-25}\ \mathrm{cm}^2 \,. \tag{9}$$

The total scattered radiation $I(x, y)$ can then be calculated by integrating over the source locations of the photons (the photosphere) and the scattering electrons (with a 3D distribution $n_e(x, y, z)$) along the line-of-sight $z$, as a function of the scattering angle $\chi(x, y, z)$ with respect to the observers line-of-sight, which was first calculated by Minnaert (1930), van de Hulst (1950), and Billings (1966). For a recent review see Howard and Tappin (2009a). The degree of polarization $p$, which is observed in the *polarized brightness (pB)* component of white-light images, is defined as,

$$p = \frac{I_T - I_R}{I_T + I_R} = \frac{I_P}{I_{\mathrm{tot}}} \,, \tag{10}$$

where $I_T$ and $I_R$ represent the tangential and radial terms of the total scattered radiation, as given in Minnaert (1930), van de Hulst (1950), Billings (1966), or Howard and Tappin (2009a). Many

# CME Mass Determination from EUV Dimming

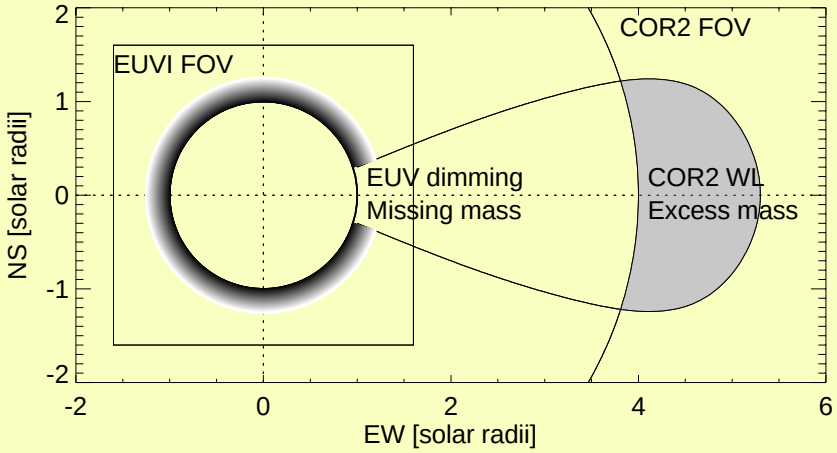


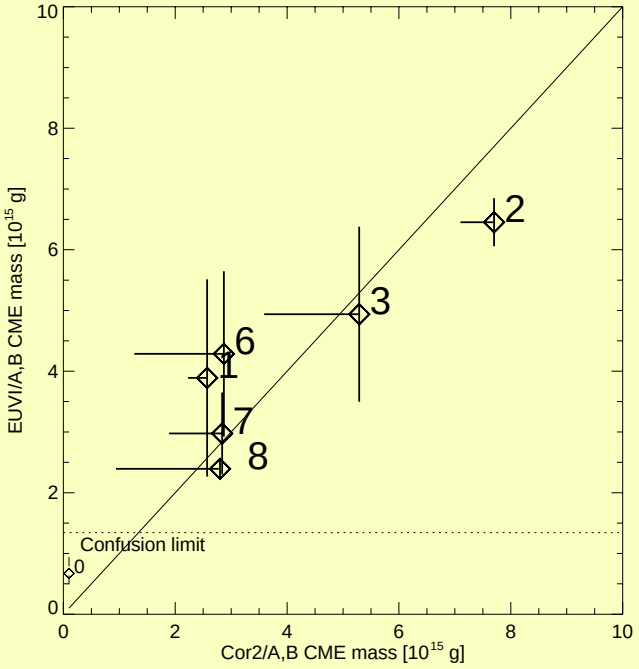


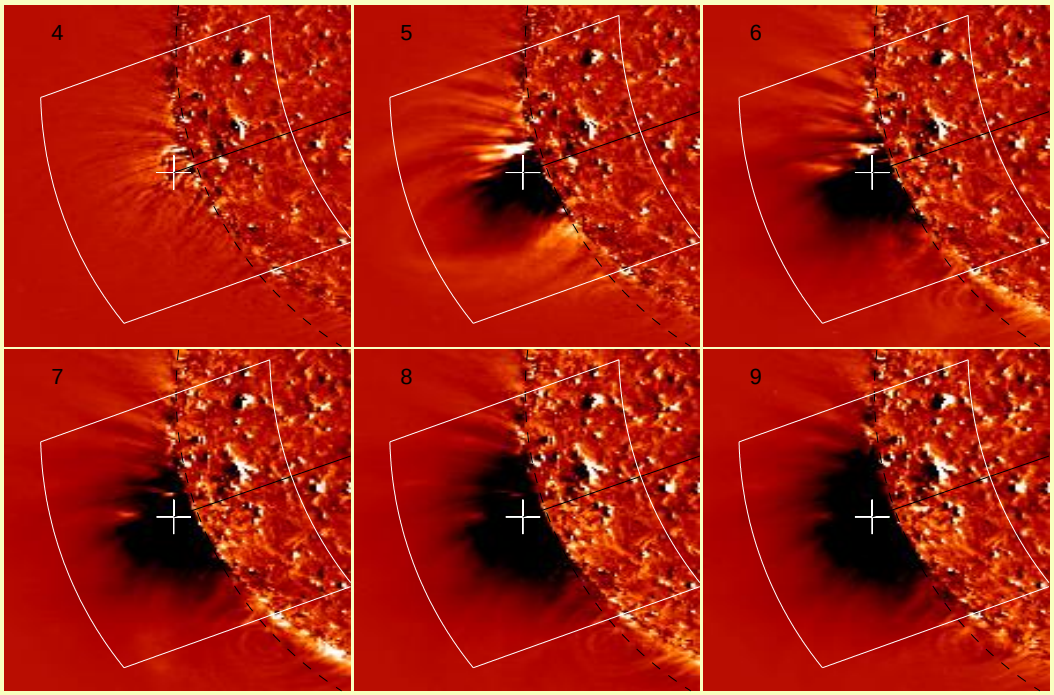


Aschwanden et al. (2009)
ApJ 706, 376

# Geometry of CME-related Dimming Volume

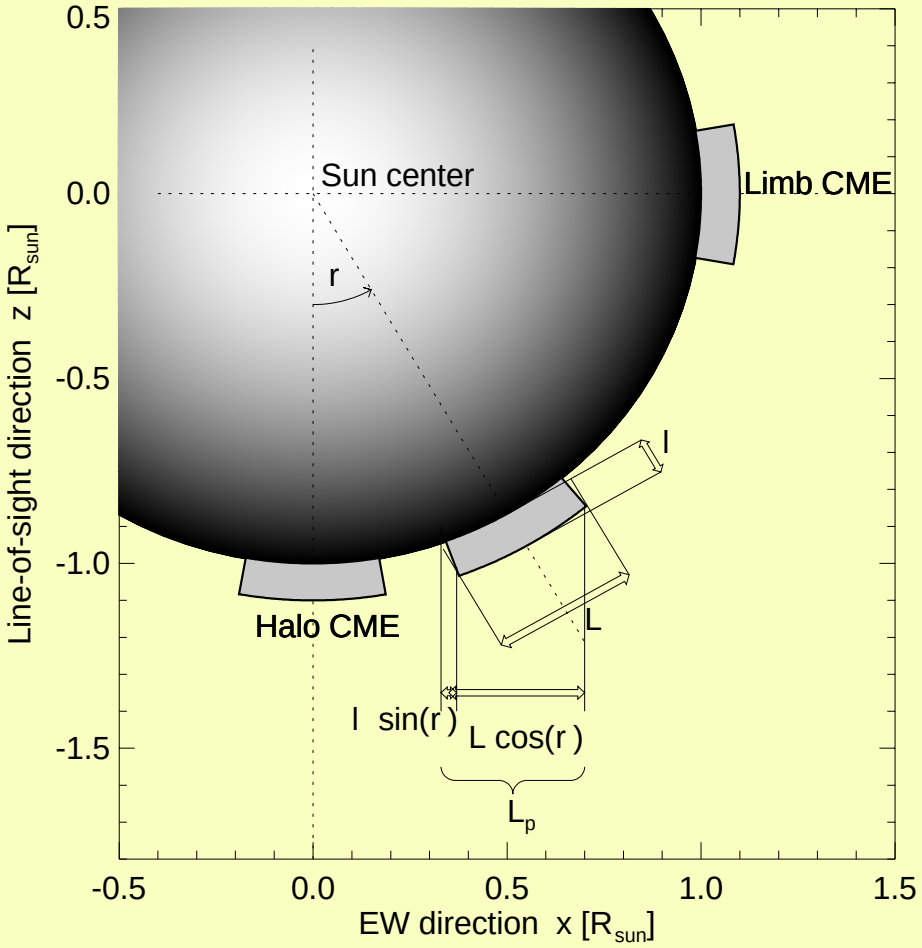


Dimming volume $V$ ($A$=area, $L$=length cale, $\lambda$=scale height):

$$V = A\lambda = L^2\lambda \ ,$$

Unforeshortened area:

$$A = L^2 \ .$$

Observed area $A_p$ (projected along line-of-sight):

$$A_p = L\ L_p \ ,$$

Foreshortened length scale $L_p$:

$$L_p = L\cos(\rho) + \lambda\sin(\rho) = \frac{A_p}{L} \ ,$$

Heliographic position (l=longitude, b=latitude):

$$\cos(\rho) = cos(l)\cos(b) \ ,$$

Unforeshortened length scale $L$:

$$L = \frac{-\lambda\ \sin(\rho) \pm \sqrt{\lambda^2\sin^2(\rho) + 4A_p\cos(\rho)}}{2\cos(\rho)}$$

Correction for center-limb variation of dimming area and volume

# CME Radial Adiabatic Expansion Model



CME at limb

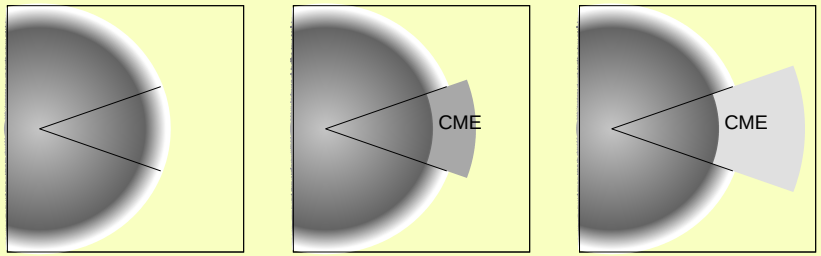


CME at disk center

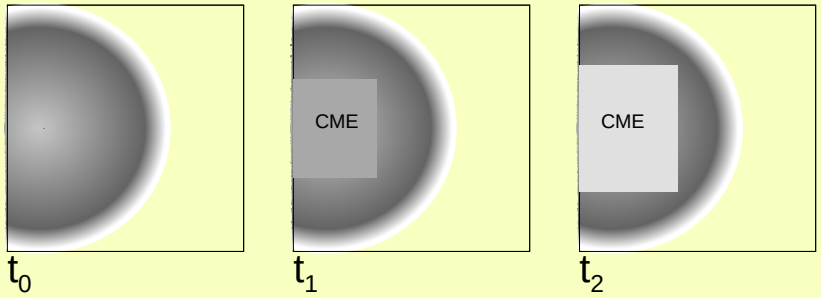


Observables:

- Emission measure dEM(x,y,T)
- Dimming area A
- EUV dimming curve EM(t)

Spatial-Synthesis Differential Emission Measure (DEM) of CME:

$$\frac{\mathrm{d}EM(T,x,y)}{\mathrm{d}T} = EM_p(x,y)\exp\left(-\frac{[\log(T)-\log(T_p(x,y))]^2}{2\sigma_T^2(x,y)}\right) ,$$

Total space and temperature-integrated emission measure of CME:

$$EM_{\mathrm{tot}} = \int\int\int \frac{\mathrm{d}EM(T,x,y)}{\mathrm{d}T}\, dT\, dx\, dy \; .$$

$$EM_{\mathrm{tot}} = \int n_e^2(\mathbf{x})\, dV = n_e^2 V = n_e^2 L^2 \lambda \; ,$$

Mean electron density $n_e$ in CME source region:

$$n_e = \sqrt{\frac{EM_{\mathrm{tot}}}{L^2\lambda}} \; .$$

CME mass:

$$m_{\mathrm{cme}} = n_e\, m_p\, V = n_e\, m_p\, L^2\lambda \; .$$

Radial Expansion of CME:

$$\frac{V(t)}{V_0} = \frac{[R_\odot + h(t)]^3 - R_\odot^3}{[R_\odot + h_0]^3 - R_\odot^3} \; .$$

Adiabatic expansion model (density reciprocal to volume):

$$EM(t) \propto n_e(t)^2 V(t) \propto V(t)^{-1} \; ,$$

Mormalized emission measure ratio $q_{EM}(t)$,

$$q_{EM}(t) = \frac{EM(t)}{EM_0)} = \frac{[R_\odot + h_0]^3 - R_\odot^3}{[R_\odot + h(t)]^3 - R_\odot^3} \; .$$

Background correction of emission measure:

$$EM(t) = EM_{\mathrm{max}}[q_{\mathrm{bg}} + (1 - q_{\mathrm{bg}})q_{\mathrm{EM}}(t)] \; ,$$

# CME Kinematics

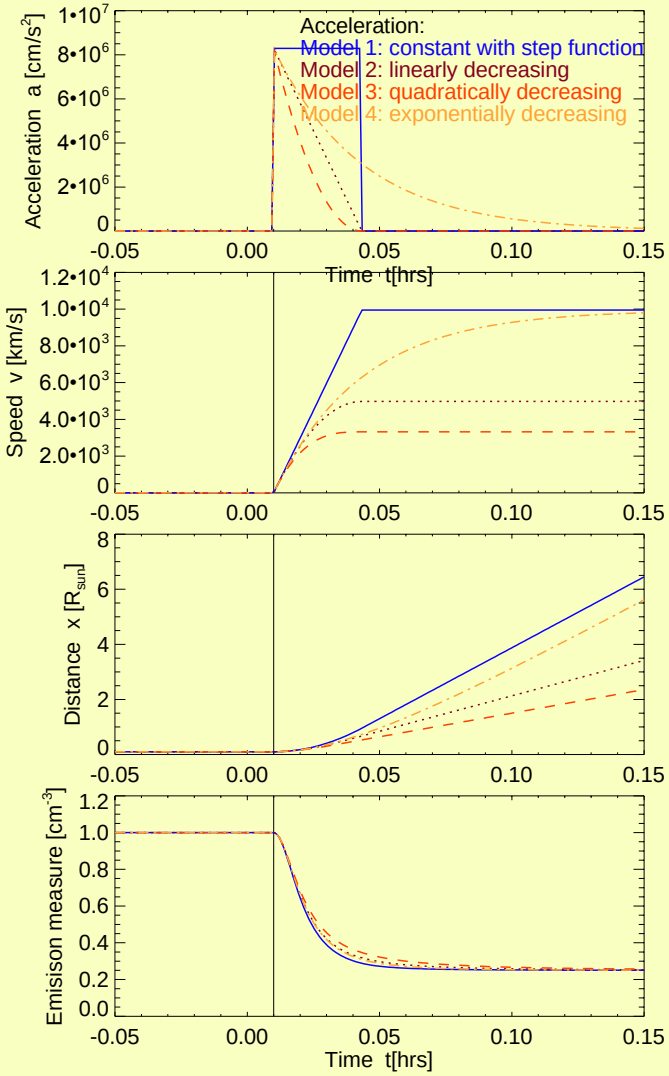


Acceleration $a(t)$:

$$a(t) = \begin{cases} a_0 & \text{for } t_0 < t < t_A \quad \text{(Model 1)} \\ a_0(1-(t-t_0)/\tau) & \text{for } t_0 < t < t_A \quad \text{(Model 2)} \\ a_0(1-(t-t_0)/\tau)^2 & \text{for } t_0 < t < t_A \quad \text{(Model 3)} \\ a_0 \exp\left[-(t-t_0)/\tau\right] & \text{for } t_0 < t < t_A \quad \text{(Model 4)} \end{cases}$$

Velocity profile $v(t)$:

$$v(t) = \int_{t_0}^{t} a(t)\ dt = \begin{cases} a_0(t-t_0) & \text{for } t_0 < t < t_A \quad \text{(Model 1)} \\ a_0[(t-t_0-(t-t_0)^2/2\tau] & \text{for } t_0 < t < t_A \quad \text{(Model 2)} \\ (1/3)a_0\tau[1-(1-(t-t_0)/\tau)^3] & \text{for } t_0 < t < t_A \quad \text{(Model 3)} \\ a_0\tau[1-\exp(-(t-t_0)/\tau)] & \text{for } t_0 < t < t_A \quad \text{(Model 4)} \end{cases}$$

Velictiy at times after the acceleration phase ($t > t_A$):

$$v(t) = \int_{t_0}^{t} a(t)\ dt = \begin{cases} a_0\tau & \text{for } t > t_A \quad \text{(Model 1)} \\ (1/2)a_0\tau & \text{for } t > t_A \quad \text{(Model 2)} \\ (1/3)a_0\tau & \text{for } t > t_A \quad \text{(Model 3)} \\ a_0\tau[1-\exp(-(t-t_0)/\tau)] & \text{for } t > t_A \quad \text{(Model 4)} \end{cases}$$

Height-time profile $h(t)$:

$$x(t) = \int_{t_0}^{t} v(t)\ dt = \begin{cases} x_0 + (1/2)a_0(t-t_0)^2 & \text{for } t_0 < t < t_A \quad \text{(Model 1)} \\ x_0 + (1/3)a_0\tau^2 & \text{for } t_0 < t < t_A \quad \text{(Model 2)} \\ x_0 + (1/3)a_0\tau[(t-t_0) + (1/4)\tau[(1-(t-t_0)/\tau]^4 - 1] & \text{for } t_0 < t < t_A \quad \text{(Model 3)} \\ x_0 + a_0\tau(t-t_0) - a_0\tau^2[1-\exp(-(t-t_0)/\tau] & \text{for } t_0 < t < t_A \quad \text{(Model 4)} \end{cases}$$

Height time profile at times after the acceleration phase ($t > t_A$):

$$x(t) = \int_{t_0}^{t} v(t)\ dt = \begin{cases} x_0 + (1/2)a_0\tau^2 + a_0\tau(t-t_A) & \text{for } t > t_A \quad \text{(Model 1)} \\ x_0 + (1/3)a_0\tau^2 + (1/2)a_0\tau(t-t_A) & \text{for } t > t_A \quad \text{(Model 2)} \\ x_0 + (1/4)a_0\tau^2 + (1/3)a_0\tau(t-t_A) & \text{for } t > t_A \quad \text{(Model 3)} \\ x_0 + a_0\tau(t-t_0) - a_0\tau^2[1-\exp(-(t-t_0)/\tau] & \text{for } t > t_A \quad \text{(Model 4)} \end{cases}$$

## Fitting of CME kinematics to observed dimming profile EM(t)

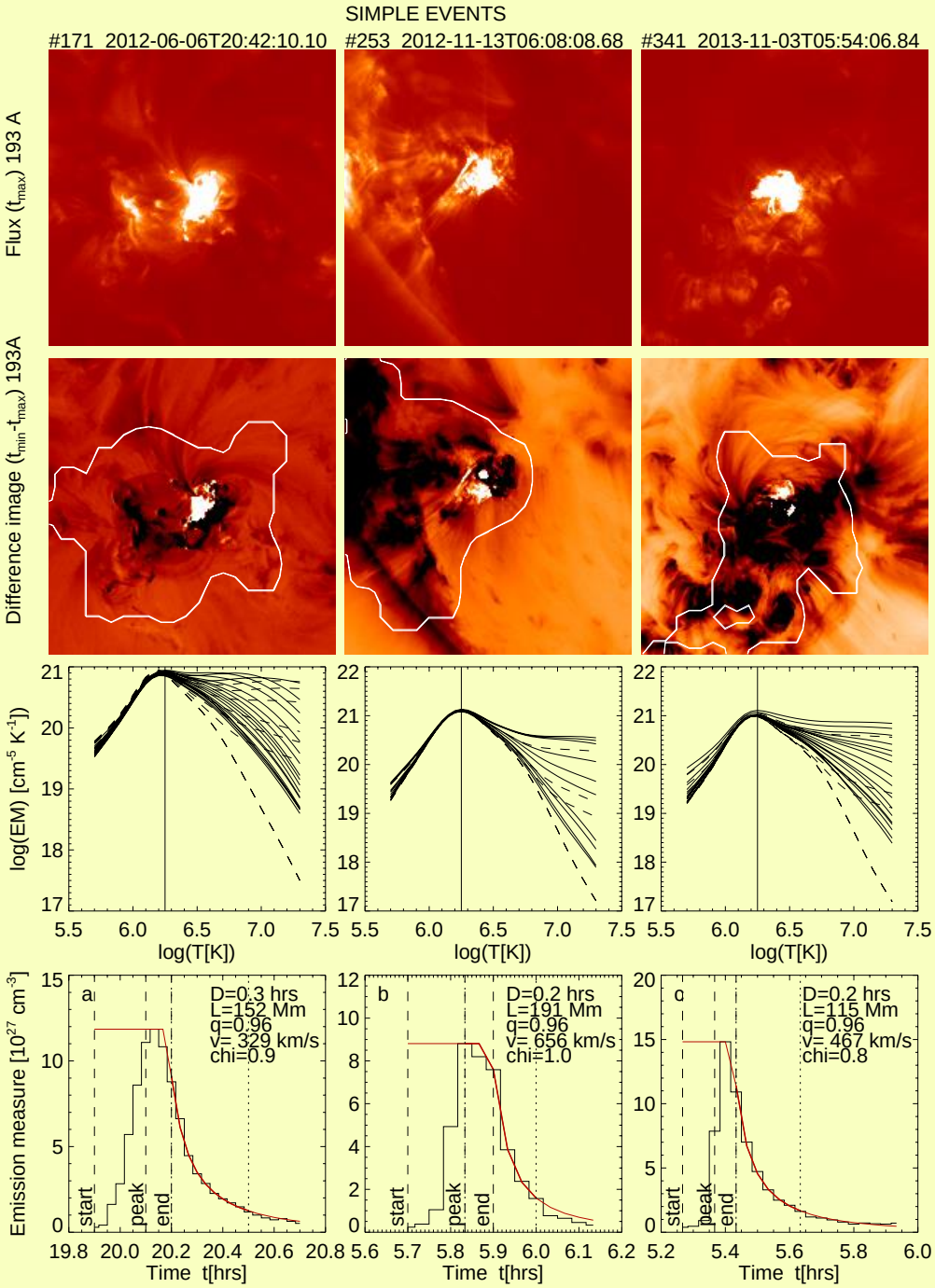


## Three examples of analyzed flares:

(a) Flux $I_{193}(x,y)$
(b) Difference image with dimming area
(c ) Emission measure DEM(T)
(d) EUV dimming profile of total emission measure EM(t)

The total emission measure Includes all emission in the Temperature range of 0.5-20 MK

→ Dimming is a density rarification and not a cooling effect !

# Statistics of CME and dimming parameters

Table 1. Ranges and distributions of CME parameters measured in 399 CME events with AIA. The mean and standard deviations refer to the slopes $p$ of power law distributions, or to the Gaussian normal distributions $x \pm \sigma_x$. The dimming delay is defined as the time difference $\Delta t = (t_{\rm dimm} - t_{\rm peak})$ between the beginning of EUV dimming and the GOES (1-8 Å) flare peak time.

| Parameter | Range | Distribution type | Mean and standard deviation |
|---|---|---|---|
| Length scale $L$ | (28...361) Mm | power law | $p = -3.4 \pm 1.0$ |
| Projected area $A_p$ | $(0.2...4.0) \times 10^{20}$ cm$^2$ | power law | $p = -1.3 \pm 0.1$ |
| CME dimming area $A$ | $(0.1...13.0) \times 10^{20}$ cm$^2$ | power law | $p = -1.3 \pm 0.1$ |
| CME dimming volume $V$ | $(0.06...12) \times 10^{30}$ cm$^3$ | power law | $p = -2.5 \pm 0.6$ |
| Dimming time $\tau_{\rm dimm}$ | (0.5...33) min | power law | $p = -2.5 \pm 0.6$ |
| Propagation time $\tau_{\rm prop}$ | (0.3...54) min | power law | $p = -1.5 \pm 0.2$ |
| GOES flare duration | (0.1...7.0) hrs | power law | $p = -2.0 \pm 0.2$ |
| CME mass $m$ | $(0.1...30) \times 10^{15}$ erg | power law | $p = -2.2 \pm 0.5$ |
| CME emission measure $EM$ | $(2.7...334) \times 10^{27}$ cm$^{-3}$ | power law | $p = -2.4 \pm 0.5$ |
| CME speed $v$ | (26...4100) km s$^{-1}$ | power law | $p = -1.9 \pm 0.3$ |
| CME kinetic energy $E_{\rm kin}$ | $(0.003...960) \times 10^{30}$ erg | power law | $p = -1.4 \pm 0.1$ |
| CME grav. energy $E_{\rm grav}$ | $(0.2...57) \times 10^{30}$ erg | power law | $p = -2.0 \pm 0.4$ |
| CME total energy $E_{\rm tot}$ | $(0.25...1000) \times 10^{30}$ erg | power law | $p = -2.0 \pm 0.3$ |
| Dimming delay $\Delta\tau_{\rm dimm}$ | $\Delta\tau_{\rm dimm} = (-7...108)$ min | Gaussian | $\Delta\tau = 5.8 \pm 7.3$ min |
| pre-CME density $n_e$ | $(0.6...6.8) \times 10^9$ cm$^{-3}$ | Gaussian | $n_e = (1.3 \pm 0.6) \times 10^9$ cm$^{-3}$ |
| pre-CME temperature $T_e$ | (1.2...5.0) MK | Gaussian | $T_e = 1.8 \pm 0.3$ MK |
| Density scale height $\lambda$ | $\lambda = (47...235)$ Mm | Gaussian | $\lambda = 86 \pm 12$ Mm |
| Dimming fraction $q_{\rm dimm}$ | $q_{\rm dimm} = (0.3...1.0)$ | Gaussian | $q_{\rm dimm} = 0.82 \pm 0.12$ |
| Goodness-of-fit $\chi$ | (0.06...6.1) | Gaussian | $\chi = 1.6 \pm 1.1$ |

# Simple and complex EUV dimming events

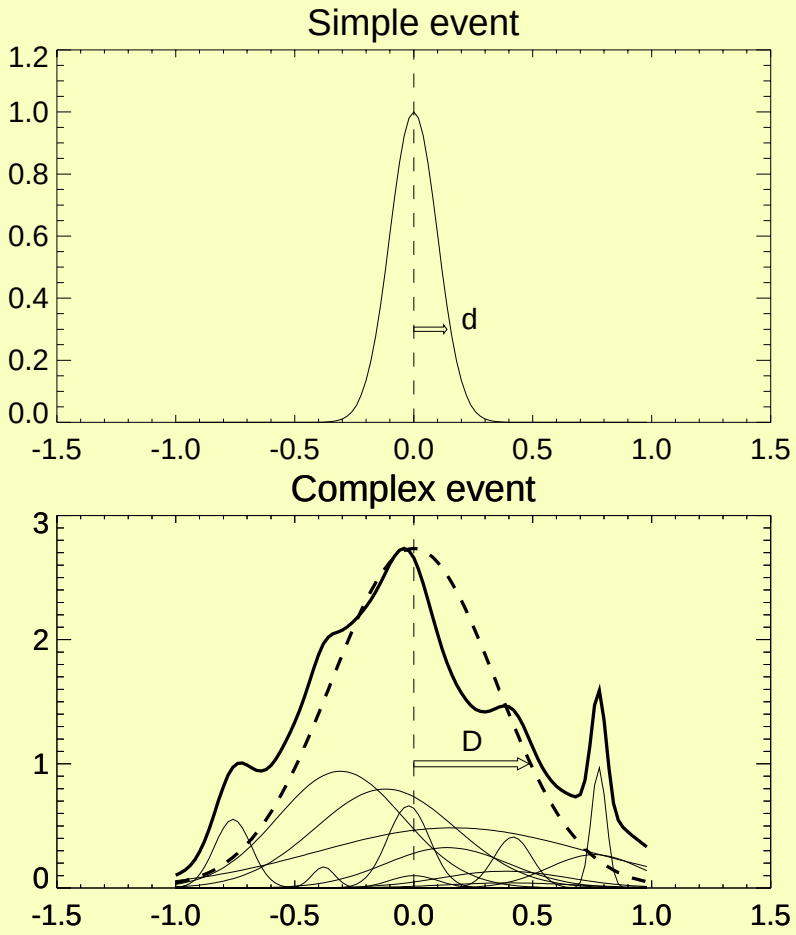


Complex events consist of multiple time-delayed dimming episodes. Fitting of complex events with single adiabatic expansion model underestimates CME speed !

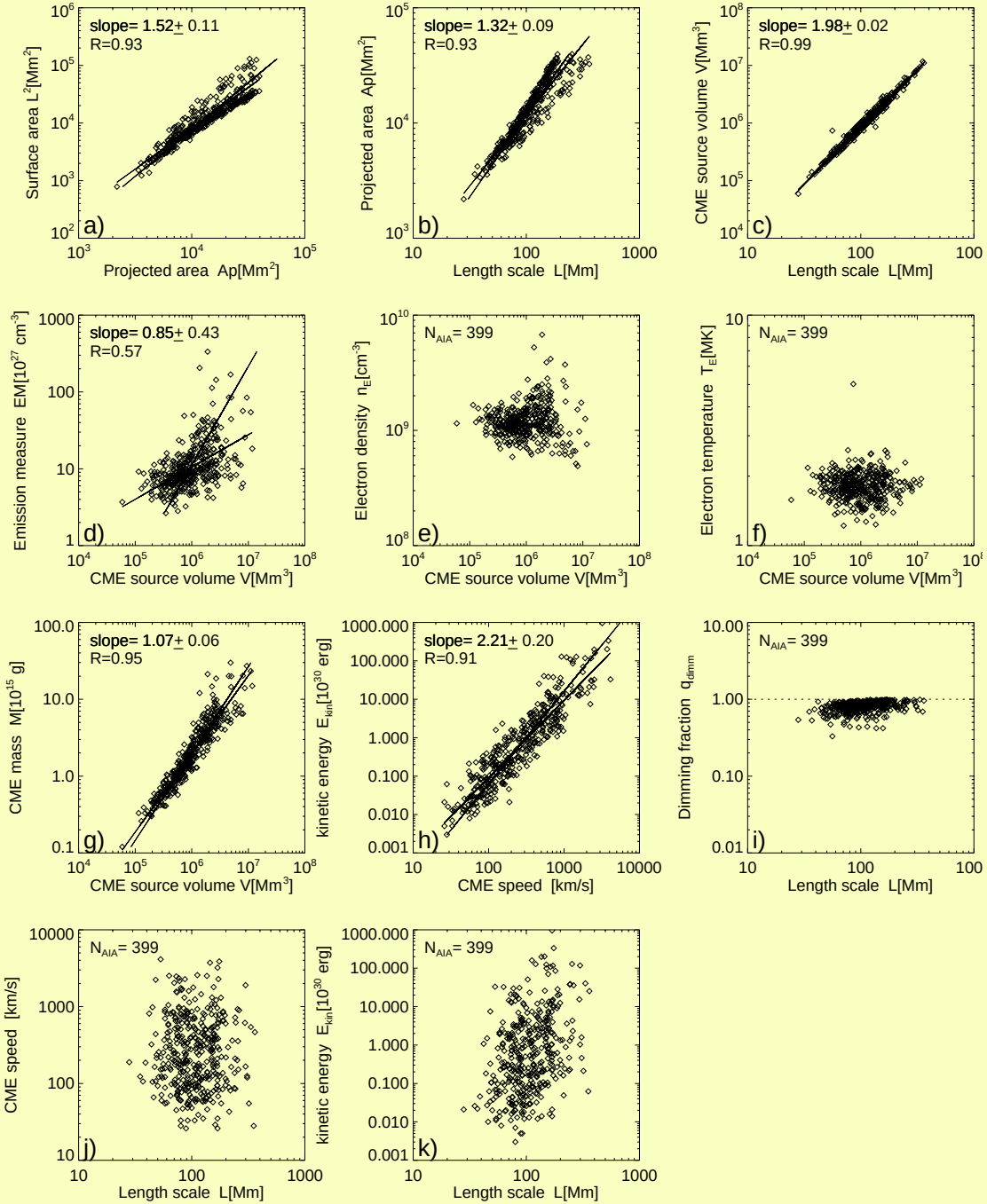


Correlations of EUV dimming parameters

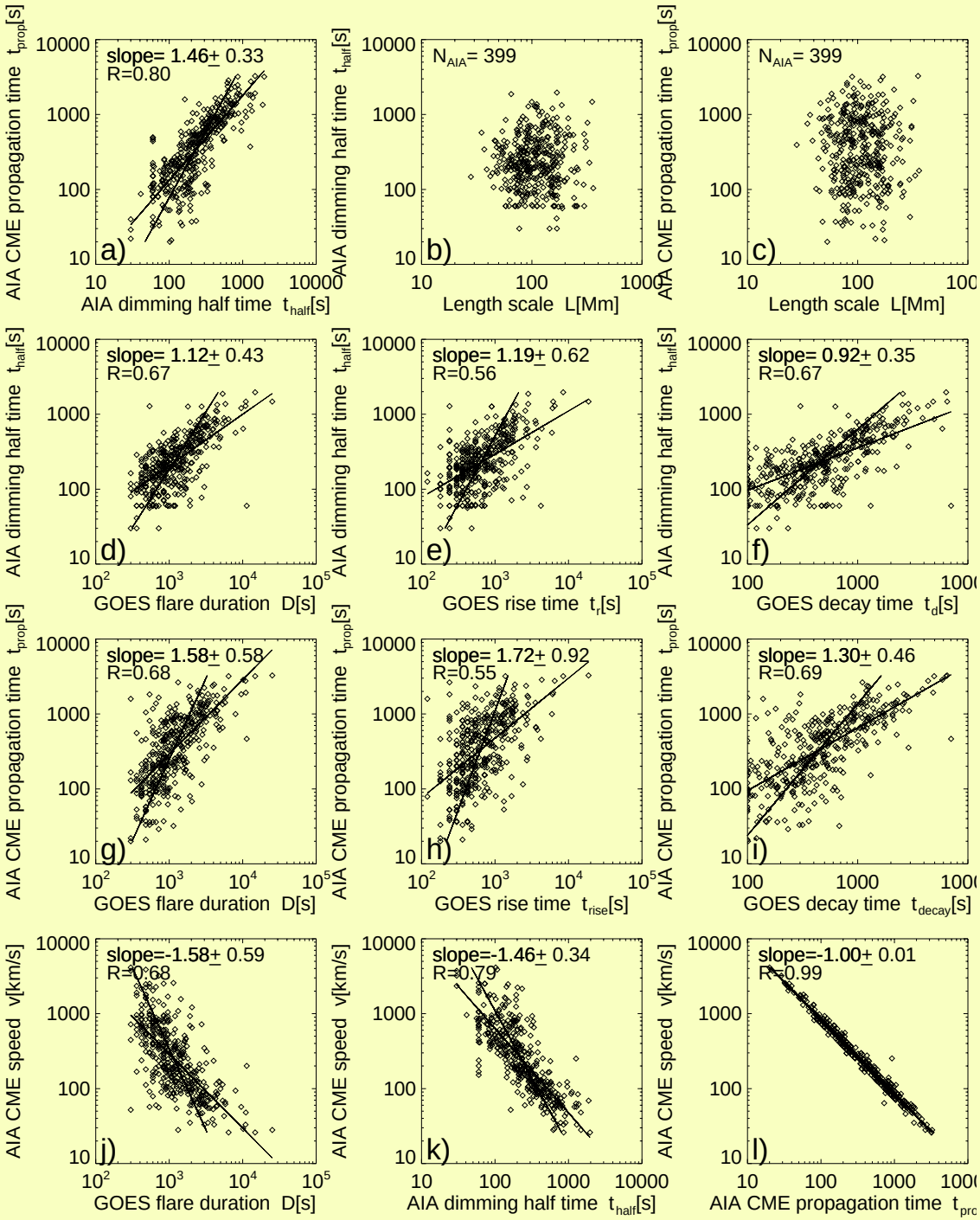


[Correlations of GOES and AIA Temporal parameters]

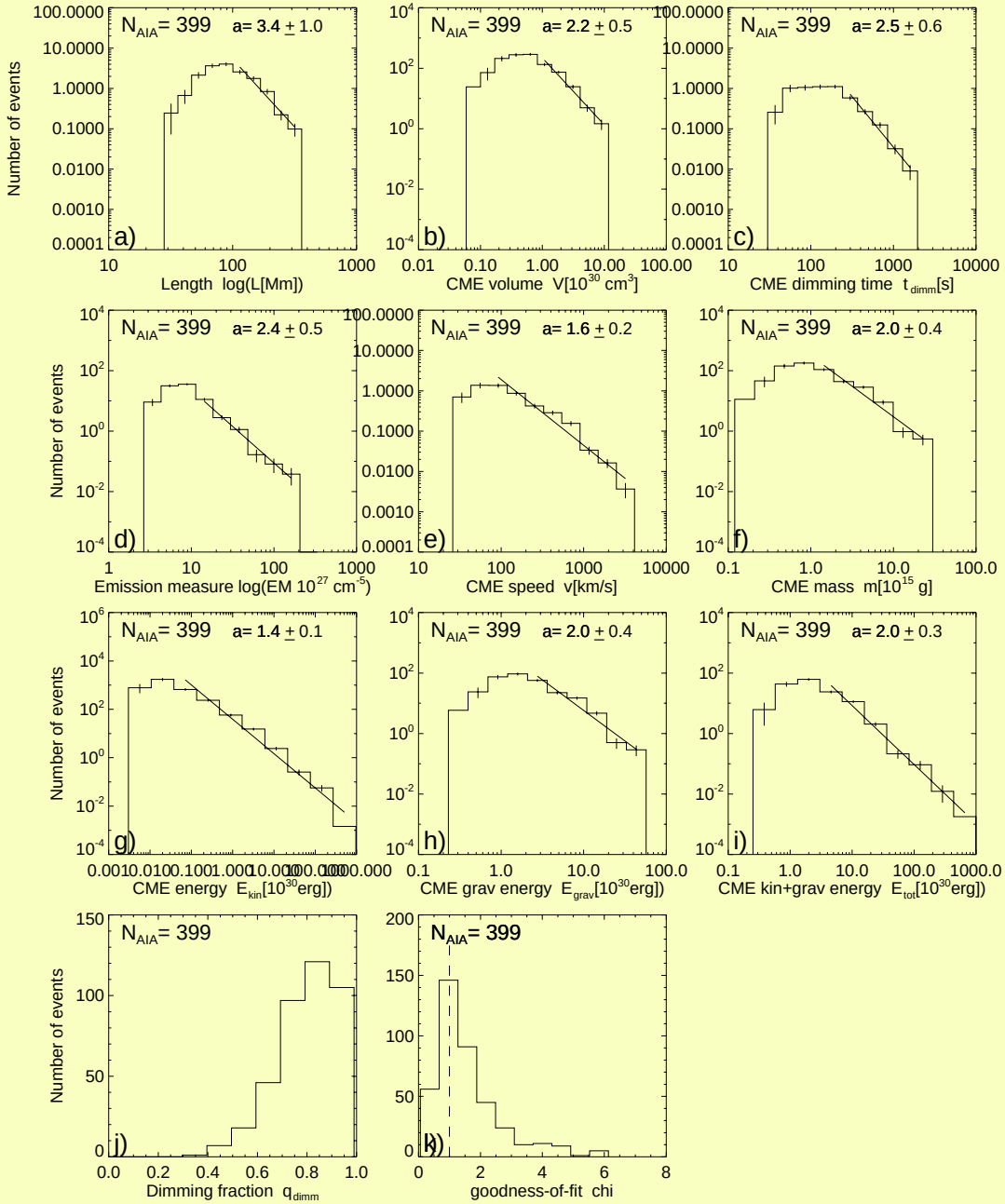


Power Law size distributions of CME parameters measured in 399 flare events Observed with AIA

# Size distributions of CME and dimming parameters

Table 1. Predicted and observed occurrence frequency distributions $N(x)$ and correlations $x \propto y^p$ of CME parameters.

| Parameter | Function | Theoretical Exponent | Observed Exponent | Reference Figure |
|---|---|---|---|---|
| Length scale $L$ | $N(L) \propto L^d$ | $d = -3.0$ | $d = -3.4 \pm 1.0$ | (Fig. 16a) |
| CME volume $V$ | $V \propto L^a$ | $a = -2.0$ | $a = -1.98 \pm 0.02$ | (Fig. 14c) |
| | $N(V) \propto V^p$ | $p = -2.2$ | $p = -2.2 \pm 0.5$ | (Fig. 16b) |
| CME mass $m$ | $m \propto V^a$ | $a = +1.0$ | $a = +1.07 \pm 0.06$ | (Fig. 14g) |
| | $N(m) \propto m^p$ | $p = -2.2$ | $p = -2.0 \pm 0.4$ | (Fig. 16f) |
| Emission measure $EM$ | $EM \propto V^a$ | $a = +1.0$ | $a = +0.9 \pm 0.4$ | (Fig. 14d) |
| | $N(EM) \propto EM^p$ | $p = -2.2$ | $p = -2.4 \pm 0.5$ | (Fig. 16d) |
| Duration $D$ | $D \propto L^a$ | $a = +2.0$ | .... | |
| | $N(D) \propto D^p$ | $p = -2.2$ | $p = -2.4 \pm 0.6$ | (Fig. 16c) |
| CME speed $v$ | $v \propto D^a$ | $a = -1.0$ | $p = -1.6 \pm 0.6$ | (Fig. 15g) |
| | $N(v) \propto v^p$ | $p = -1.8$ | $p = -1.9 \pm 0.2$ | (Fig. 16e) |
| CME kinetic energy $E_{\rm kin}$ | $E_{\rm kin} \propto v^a$ | $a = +2.0$ | $p = +2.2 \pm 0.2$ | (Fig. 14h) |
| | $N(Ek) \propto Ek^p$ | $p = -1.4$ | $p = -1.4 \pm 0.1$ | (Fig. 16g) |
| CME grav. energy $E_{\rm grav}g$ | $E_{\rm grav} \propto m^a$ | $a = +1.0$ | | |
| | $N(Eg) \propto Eg^p$ | $p = -2.2$ | $p = -2.0 \pm 0.4$ | (Fig. 16h) |
| CME total energy $E_{\rm tot}t$ | $E_{\rm tot} \propto Ek + Eg$ | | | |
| | $N(Et) \propto Et^p$ | $p = -1.9$ | $p = -2.0 \pm 0.3$ | (Fig. 16i) |

The power law slopes are consistent with the fractal-diffusive self-organized criticality model (Aschwanden 2012).

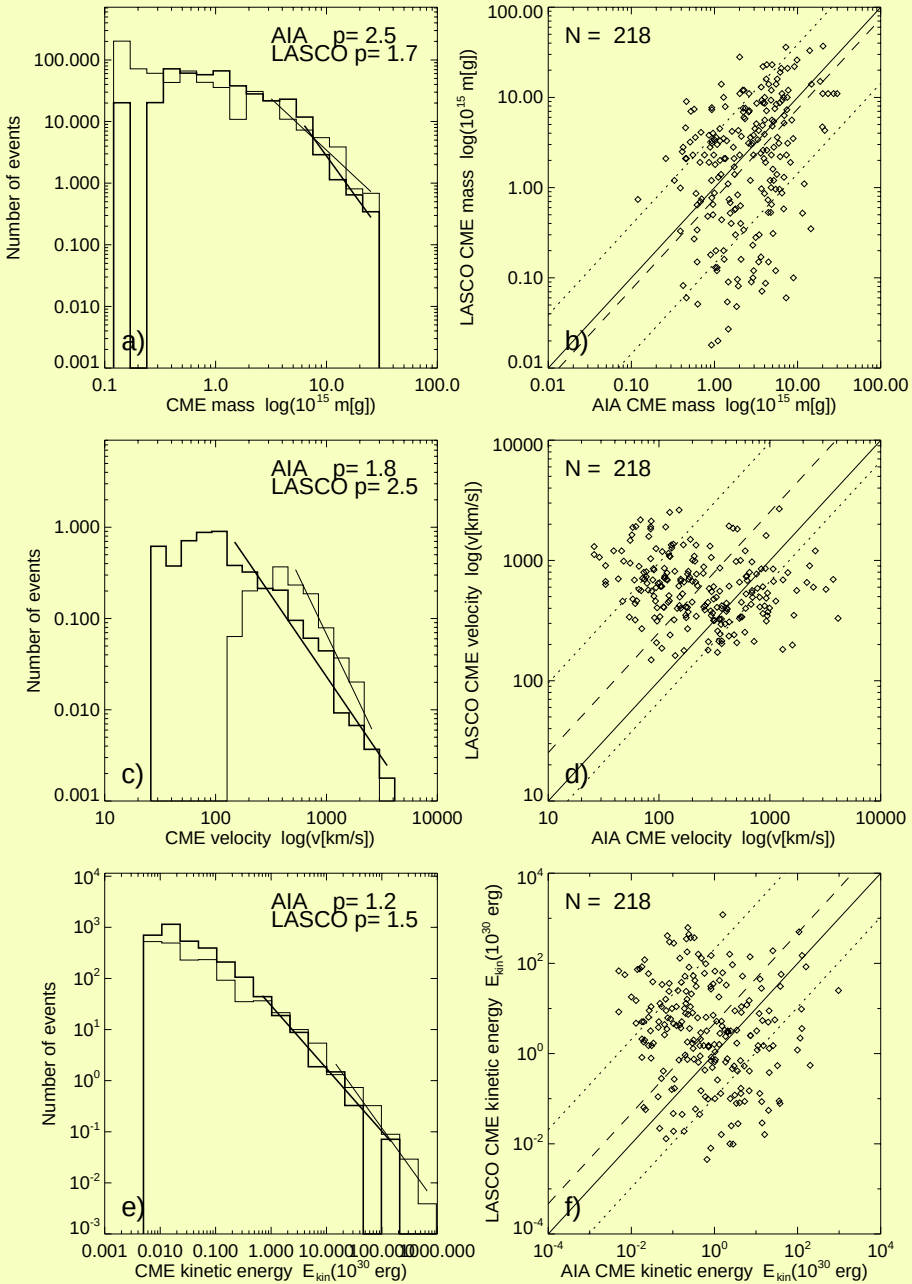


Comparison of CME masses, speeds, and energies LASCO/C2 vs. AIA

# Time delay in dimming events simultaneously observed with LASCO/C2 and AIA

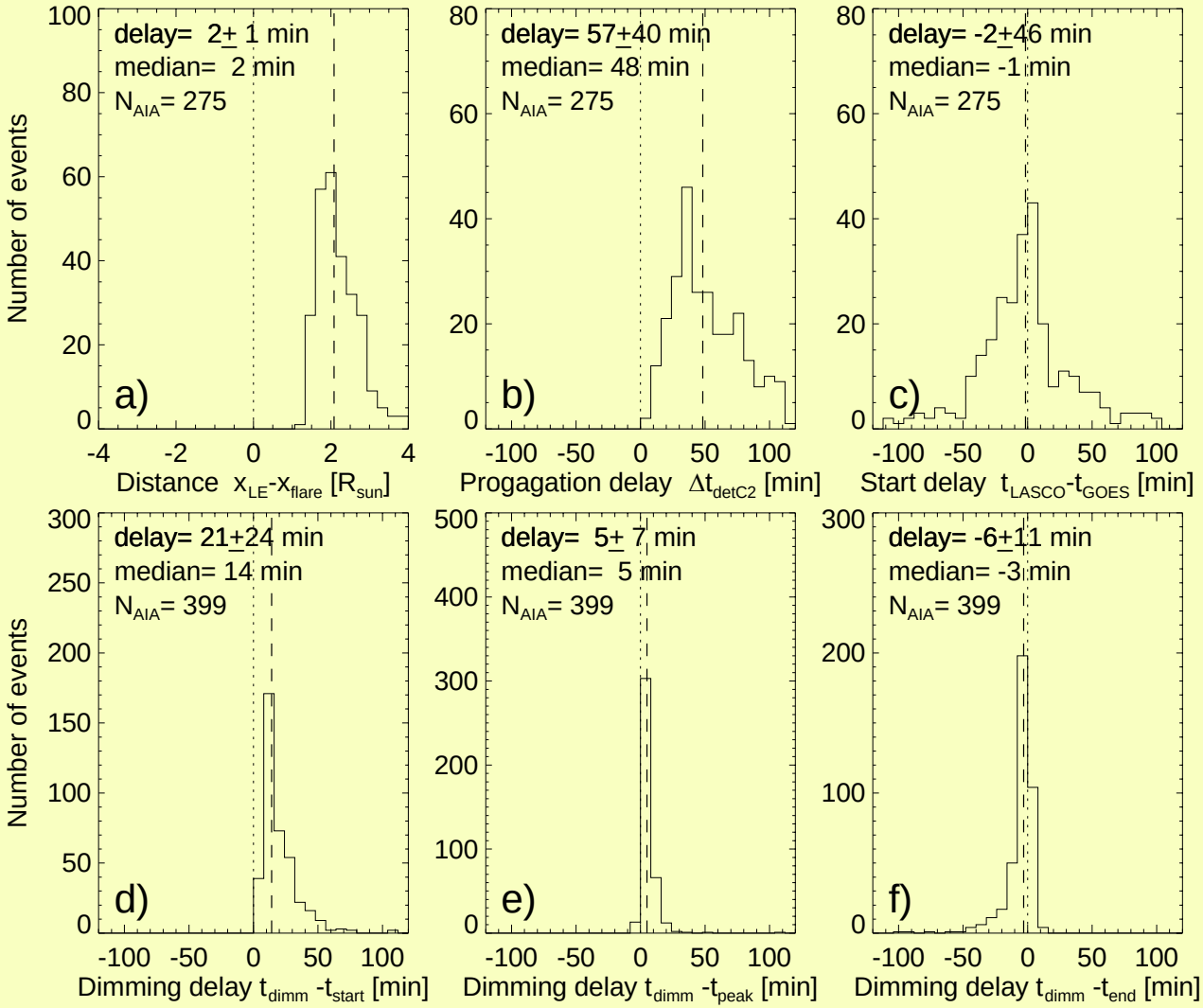


Relative timing of EUV dimming start with GOES flare peak is dt=5±7 minutes

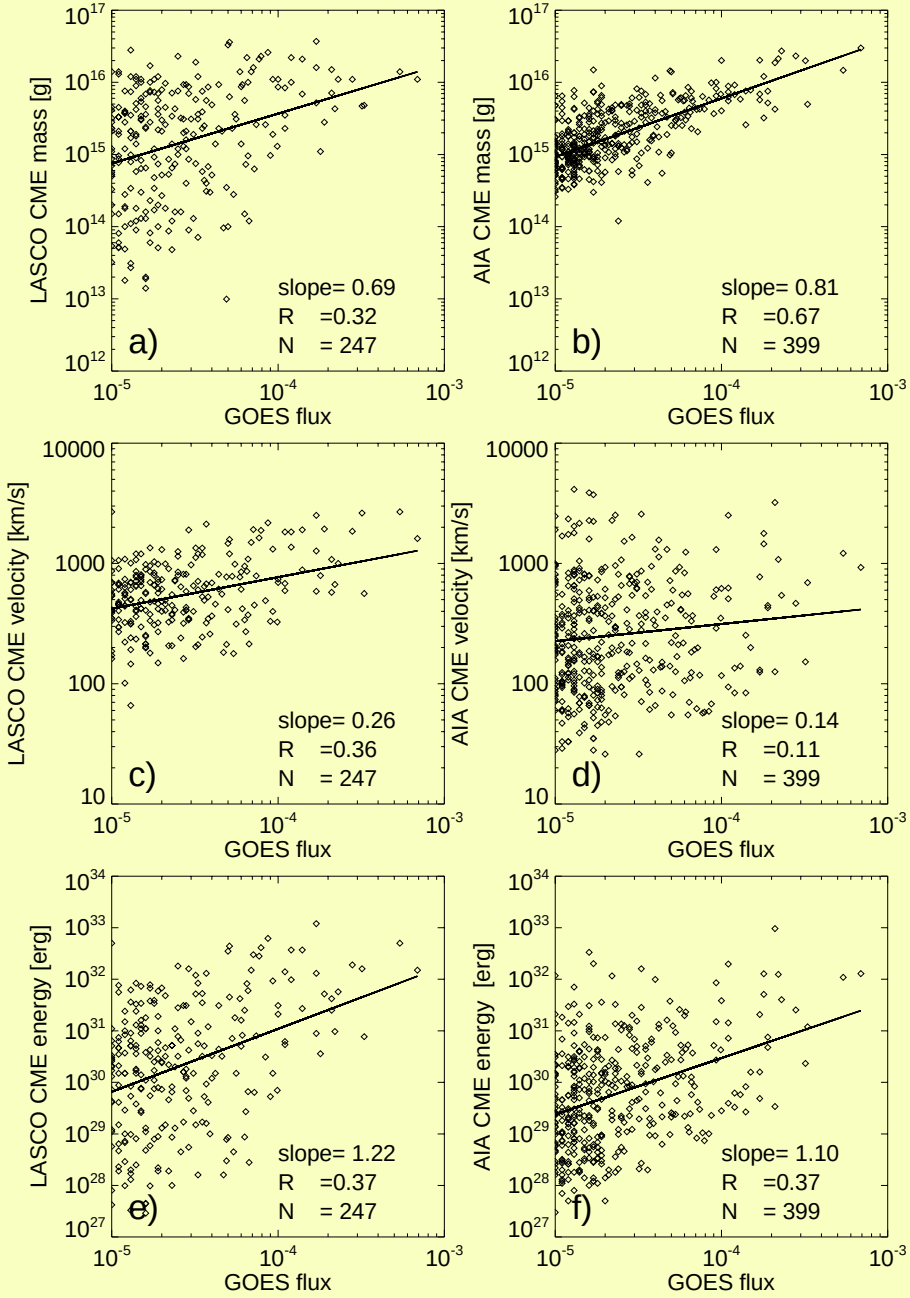


Comparison of CME masses, speeds, and energies of LASCO/C2 and AIA with GOES flare magnitude

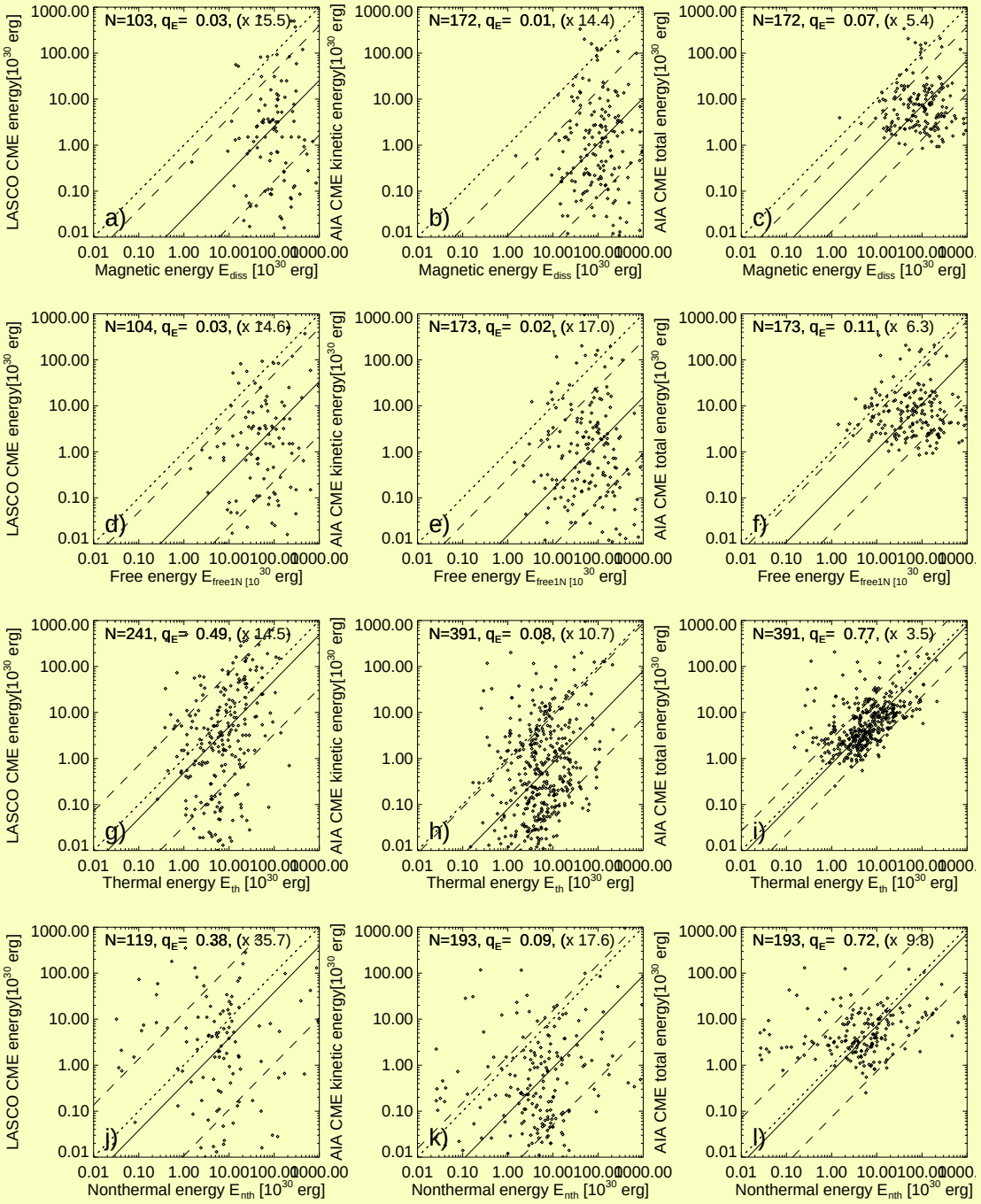


Comparison of CME kinetic energies, (LASCO/C2 and AIA) and total kinetic plus gravitational energy with magnetic, free, thermal, nonthermal energies

Including the gravitational energy to kinetic CME energy yields the log means:

$E_{CME}$ = 7% $E_{mag}$
= 11% $E_{free}$
= 77% $E_{th}$
= 72% $E_{nth}$

# Comparison of this Global Flare Energetics Survey With study of Emslie et al. (2012)

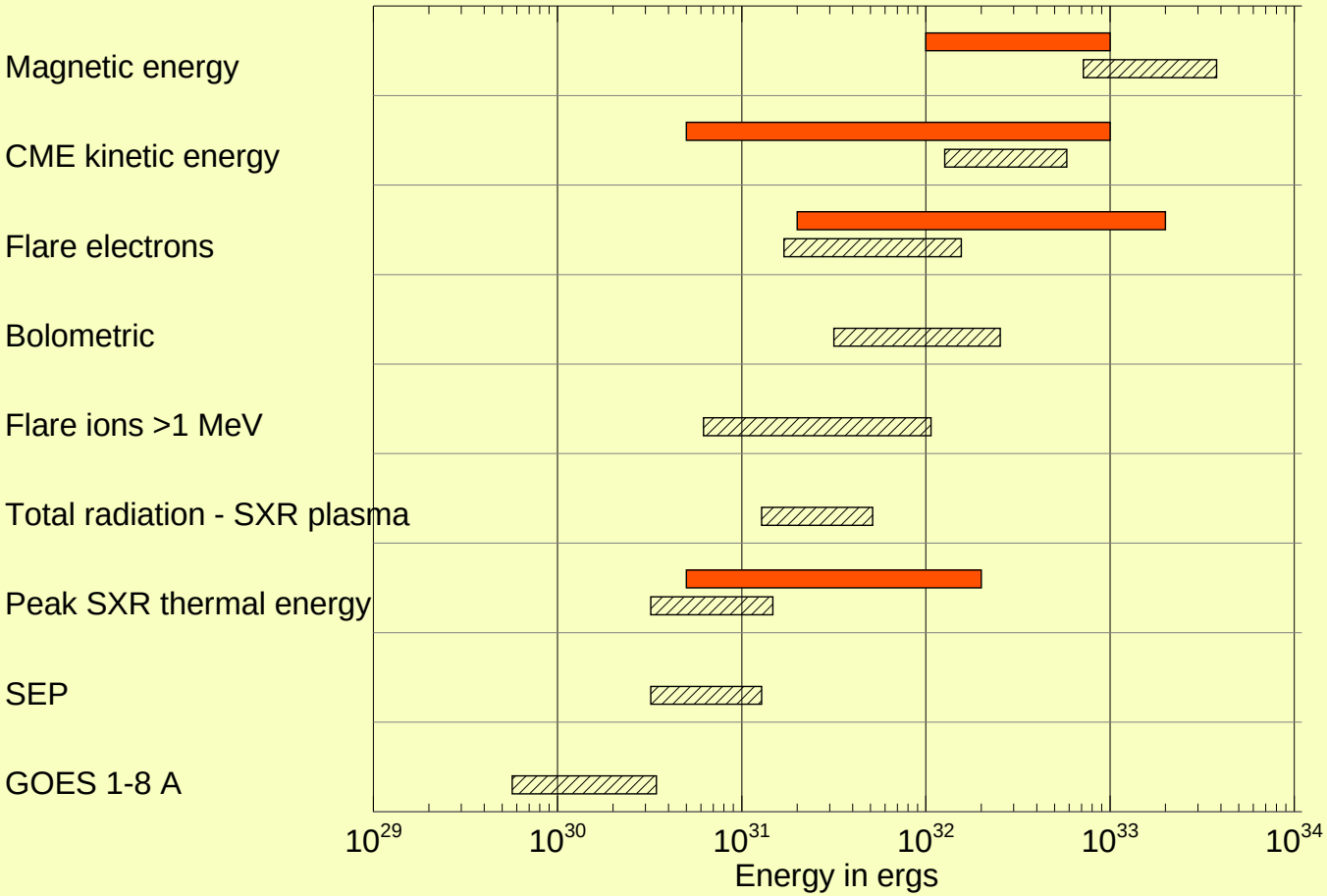


New: Magnetic energy calculated with vertical-current NLFFF, instead ad hoc
CME energy calculated from EUV dimming (AIA), instead coronagraph
Multi-thermal (spatial-synthesis DEM), instead of iso-thermal

# Conclusions :

1) The “Global Flare and CME Energetics” project entails all (399) M and X-class flares observed with SDO during the first 3.5 years of its mission and has been completed for 4 different forms of energies: magnetic energies (Paper I), thermal energies (Paper II), non-thermal energies (Paper III), and CME energies (Paper IV).

2) The (logarithmic) mean ratio between different energy conversions are:
   $E_{th} = 0.07\ E_{mag}$ → Magnetic energy is sufficient to produce thermal flare energy
   $E_{nth} = 0.07\ E_{mag}$ → Magnetic energy is sufficient to accelerate electrons
   $E_{CME} = 0.07\ E_{mag}$ → Magnetic energy is sufficient to launch CME

3) The (logarithmic) mean ratio between thermal and non-thermal energies are:
   $E_{th} = 0.7\ E_{nth}$ → Thick-target model fails in 40% to explain thermal energy. Other forms of heating are additionally required (thermal conduction fronts, direct heating, wave heating).

4) CME energies determined in white-light with LASCO/C2 are based on leading edge speed, while EUV dimming from AIA data measures bulk velocities, which are smaller than leading edge speed, in particular in complex events.

5) Power law slopes of size distributions of all energy parameters can be modeled with self-organized criticality models.

*http://www.lmsal.com/~aschwand/ppt/2016_RHESSI_Graz.ppt*
*http://www.lmsal.com/~aschwand/RHESSI/flare_energetics.html*